Nitric oxide acts as a cotransmitter in a subset of dopaminergic neurons to diversify memory dynamics

Yoshinori Aso[1]*, Robert Ray[1], Xi Long[1], Karol Cichewicz[2], Teri-TB Ngo[1], Brandi Sharp[1], Christina Christoforou[1], Andrew Lemire[1], Jay Hirsh[2], Ashok Litwin-Kumar[3], Gerald M. Rubin[1]*

[1] Janelia Research Campus, Howard Hughes Medical Institute, 19700 Helix Drive, Ashburn, VA 20147, USA

[2] Department of Biology, University of Virginia, Charlottesville, VA 22904, USA

[3]Department of Neuroscience, Columbia University, 3227 Broadway, New York, NY 10027, USA

Contact Info

Correspondence: asoy@janelia.hhmi.org and rubing@janelia.hhmi.org

Summary

Animals employ multiple and distributed neuronal networks with diverse learning rules and synaptic plasticity dynamics to record distinct temporal and statistical information about the world. However, the molecular mechanisms underlying this diversity are poorly understood. The anatomically defined compartments of the insect mushroom body function as parallel units of associative learning, with different learning rates, memory decay dynamics and flexibility (Aso & Rubin 2016). Here we show that nitric oxide (NO) acts as a neurotransmitter in a subset of dopaminergic neurons in *Drosophila*. NO's effects develop more slowly than those of dopamine and depend on soluble guanylate cyclase in postsynaptic Kenyon cells. NO acts antagonistically to dopamine; it shortens memory retention and facilitates the rapid updating of memories. The interplay of NO and dopamine enables memories stored in local domains along Kenyon cell axons to be specialized for predicting the value of odors based only on recent events. Our results provide key mechanistic insights into how diverse memory dynamics are established in parallel memory systems.

Keywords

memory dynamics, associative learning, cotransmitter, dopamine, nitric oxide, mushroom body, *Drosophila*

Introduction

An animal's survival in a dynamically changing world depends on storing distinct sensory information about their environment as well as the temporal and probabilistic relationship between those cues and punishment or reward. Thus it is not suprising that multiple distributed neuronal circuits in the mammalian brain have been shown to process and store distinct facets of information acquired during learning (White & McDonald, 2002). Even a simple form of associative learning such as fear conditioning induces enduring changes, referred to as memory engrams, in circuits distributed across different brain areas (Herry & Johansen, 2014). Do these multiple engrams serve different mnemonic functions, what molecular and circuit mechnisms underly these differences, and how are they integrated to control behavior? Localizing these distributed engrams, understanding what information is stored in each individual memory unit and how units interact to function as one network are important but highly challenging problems.

The Drosophila mushroom body (MB) provides a well-characterized and experimentally tractable system to study parallel memory circuits. Olfactory memory formation and retrieval in insects requires the MB (Debelle & Heisenberg, 1994; Dubnau, Grady, Kitamoto, & Tully, 2001; Erber, MASUHR, & MENZEL, 1980; Heisenberg, 2003; McGuire, Le, & Davis, 2001). In associative olfactory learning, exposure to an odor paired with a reward or punishment results in formation of a positive- or negative-valence memory, respectively (Quinn, Harris, & Benzer, 1974; Tempel, Bonini, Dawson, & Quinn, 1983; Tully & Quinn, 1985). In the MB, sensory stimuli are represented by the sparse activity of ~2,000 Kenyon cells (KCs). Each of 20 types of dopaminergic neurons

(DANs) innervates compartmental regions along the parallel axonal fibers of the KCs. Similarly, 22 types of mushroom body output neurons (MBONs) arborize their dendrites in specific axonal segments of the KCs; together, the arbors of the DANs and MBONs define the compartmental units of the MB (Aso, Hattori, et al., 2014; Mao & Davis, 2009; Tanaka, Tanimoto, & Ito, 2008). Activation of individual MBONs can cause behavioral attraction or repulsion, depending on the compartment in which their dendrites aborize, and MBONs appear to use a population code to govern behavior (Owald et al 2015; Aso et al 2014b).

A large body of evidence indicates that these anatomically defined compartments of the MB are also the units of associative learning (Aso et al., 2012; Aso, Sitaraman, et al., 2014; Aso et al., 2010; Berry, Phan, & Davis, 2018; A. L. Blum, W. Li, M. Cressy, & J. Dubnau, 2009; Bouzaiane, Trannoy, Scheunemann, Placais, & Preat, 2015; Burke et al., 2012; Claridge-Chang et al., 2009; Huetteroth et al., 2015; Ichinose et al., 2015; Isabel, Pascual, & Preat, 2004; Krashes et al., 2009; Lin et al., 2014; Liu et al., 2012; Owald et al., 2015; Pai et al., 2013; Placais, Trannoy, Friedrich, Tanimoto, & Preat, 2013; Schwaerzel et al., 2003; Sejourne et al., 2011; Trannoy, Redt-Clouet, Dura, & Preat, 2011; Yamagata et al., 2015; Zars, Fischer, Schulz, & Heisenberg, 2000). Despite the long history of behavioral genetics in fly learning and memory, many aspects of the signaling pathways governing plasticity—especially whether they differ between compartments—remain poorly understood. Nevertheless, dopaminergic neurons and signaling play a key role in all MB compartments, and flies can be trained to form associative memories by pairing the presentation of an odor with stimulation of a single dopaminergic neuron (Aso et al., 2010). Punishment or reward activates distinct sets of

DANs that innervate specific compartments of the MB (Das et al., 2014; Galili et al., 2014; Kirkhart & Scott, 2015; Liu et al., 2012; Mao & Davis, 2009; Riemensperger, Voller, Stock, Buchner, & Fiala, 2005; Tomchik, 2013). Activation of the DAN innervating a MB compartment induces enduring depression of KC-MBONs synapses in those specific KCs that were active in that compartment at the time of dopamine release (Berry et al., 2018; Bouzaiane et al., 2015; Cohn, Morantte, & Ruta, 2015; Hige, Aso, Modi, Rubin, & Turner, 2015; Owald et al., 2015; Sejourne et al., 2011). Thus, which compartment receives dopamine during training appears to determine the valence of the memory, while which KCs were active during training determines the sensory specificity of the memory (Figure 1A).

Compartments operate with distinct learning rules. Selective activation of DANs innervating specific compartments has revealed that they can differ extensively in their rates of memory formation, decay dynamics, storage capacity, and flexibility to learn new associations (Aso et al., 2012; Aso & Rubin, 2016; Huetteroth et al., 2015; Yamagata et al., 2015). For instance, the dopaminergic neuron PAM-α1 can induce a 24h memory with a single 1-minute training session, whereas PPL1-α3 requires ten repetitions of the same training to induce a 24h memory. PPL1-γ1pedc (aka MB-MP1) can induce a robust short-lasting memory with a single 10-second training, but cannot induce long-term memories even after 10 repetitions of a 1-minute training. PAM-α1 can write a new memory without compromising an existing memory, whereas PPL1-γ1pedc extinguishes the existing memory when writing a new memory (Aso & Rubin, 2016). What molecular and cellular differences are responsible for the functional diversity of these compartments? Some differences might be arise from differences among KC cell types

(reviewed in Keene and Waddel, 2007, McGuire et al., 2005), but memory dynamics are different even between compartments that lie along the axon bundles of the same Kenyon cells (for example, α1 and α3). In this paper, we show that differences in memory dynamics between compartments can arise from the deployment of distinct cotransmitters by the DAN cell types that innervate them.

Results

Dopaminergic neurons can induce memories without dopamine, but with inverted valence

DANs release diverse cotransmitters in the mammalian brain (Maher & Westbrook, 2008; Stuber, Hnasko, Britt, Edwards, & Bonci, 2010; Sulzer et al., 1998; Tecuapetla et al., 2010; Tritsch, Ding, & Sabatini, 2012). In *Drosophila*, the terminals of the MB DANs contain both clear and dense-core vesicles (Takemura et al., 2017), prompting us to ask if the DAN cell types innervating different MB compartments might use distinct cotransmitters that could play a role in generating compartment-specific learning rules. We individually activated several DAN cell types in a tyrosine hydroxylase (TH) mutant background that eliminates dopamine synthesis in the nervous system (Cichewicz et al., 2016; Riemensperger et al., 2011) and assayed their ability to induce associative learning when paired with an odor stimulus.

We first examined the PPL1 cluster of DANs, which innervate several MB compartments involved in aversive learning, driven by stimuli such as electric shock, noxious temperature, and bitter taste (Galili et al., 2014; Kirkhart & Scott, 2015; Mao & Davis, 2009; Riemensperger et al., 2005; Tomchik, 2013). Using an optogenetic olfactory arena (Aso & Rubin, 2016), we trained flies by paring odor exposure with optogenetic activation of these DANs using CsChrimson-mVenus and then immediately tested memory formation (Figure 1B, C). In flies with a wild-type TH allele, this training protocol induced robust negative-valence memory of the paired odor (Figure 1D), as observed previously (Claridge-Chang et al., 2009; Schroll et al., 2006). In the dopamine-

deficient background, activation of the same DANs still induced a robust odor memory, but its valence was now positive (Figure 1E). This result is consistent with previous findings that TH mutant flies show a weak positive-valence memory after odor-shock conditioning (Riemensperger et al., 2011), although the positive-valence memory we observed is much stronger.

Arguing against the possibility that this valence-inversion phenotype resulted from a developmental defect caused by the constitutive absence of dopamine (Niens et al., 2017), feeding L-DOPA and carbidopa to adult-stage flies fully restored normal valence memory (Figure 1F). Nor did the valence-inversion phenotype result from lack of dopamine signaling outside the MB, as restoring TH expression specifically in the PPL1 DANs was sufficient to restore formation of negative-valence memory (Figure 1G; Figure 1-figure supplement 1). Moreover, valence-inversion in the absence of dopamine was not limited to punishment-representing DANs. Activation of reward-representing PAM cluster DANs (Burke et al., 2012; Liu et al., 2012) in the TH mutant background also induced odor memory of opposite valence, in this case negative rather than positive (Figure 1D,E); as we found for PPL1-induced memories, either L-DOPA and carbidopa feeding or TH expression in reward-representing DANs restored the ability to form a memory of the valence that is observed in wild-type flies (Figure 1F,G). These observations suggested the possible presence of a cotransmitter in these DANs that exerts an opposite effect from dopamine on synaptic plasticity and memory.

Putative cotransmitter effects differ among DAN cell types

If DAN cell types use different cotransmitters, we might expect the effects of activating

158 DANs in the TH mutant background to vary with cell type. We tested this idea by
159 comparing the associative memories formed in wild-type and TH mutant backgrounds
160 when an odor was paired with optogenetic activation of different subsets of DAN cell
161 types using seven split-GAL4 driver lines (Figure 2 and Figure 2-figure supplement 1).
162 We also demonstrated that valence inversion is not limited to training using direct DAN
163 stimulation with CsChrimson; activating bitter taste sensory neurons using Gr66a-GAL4,
164 which activate PPL1-DANs (Das et al., 2014; Kirkhart & Scott, 2015), likewise induced
165 memories of inverted valence (Figure 2). We identified two DAN cell types that
166 exhibited the valence-inversion phenotype: PPL1-γ1pedc and PAM- γ5/PAM-β'2a. With
167 PPL1-γ1pedc stimulation, memory valence switched from negative to positive in TH
168 mutant animals. Conversely, with PAM-γ5 and PAM-β'2a stimulation, memory valence
169 flipped in the opposite direction, from positive to negative in TH mutants.

170 The valence-inversion phenotype was not, however, observed in all compartments.
171 Activation of PPL1-γ2α'1 resulted in negative-valence memory in both TH mutant and
172 wild type, suggesting a cotransmitter with the same sign of action as dopamine.
173 Activation of PPL1-α3 or PAM-β'1 in the TH mutant background did not induce
174 significant memory, indicating that these cells do not express a cotransmitter capable of
175 inducing memory without dopamine.

176 **Identification of nitric oxide synthase in a subset of DAN cell types by transcript**
177 **profiling**

178 To identify potential cotransmitters, we profiled (using RNA-Seq methods) the
179 transcriptomes of the DAN cell types in these seven split-GAL4 lines, and looked for

candidates whose expression correlated with the valence-inversion effect. Isolation of pure populations of specific DAN cell types is challenging because of their low abundance. For example, PPL1 is a single cell in each brain hemisphere and thus requires ~50,000-fold enrichment. We used a collection of split-GAL4 driver lines (Aso, Hattori, et al., 2014) to fluorescently mark the soma of specific DAN cell types and confirmed that the nuclear-targeted reporters we used for sorting visualized the same restricted set of cells as the membrane-targeted reporters in the original study. In this way, we selected a combination of reporter and driver lines that provided the most specific labeling of the targeted cell type. The number of detected genes and the correlation across biological replicates of RNA profiling experiments has been observed to be highly dependent on cDNA yield during library constuction (Fred P. Davis1, 2018). Due to different soma sizes, the amount of mRNA per cell is expected to differ across cell types. To estimate the number of cells necessary for our experimental condition, we started with MBON-γ1pedc>α/β cells, a cell type that occurs once per hemisphere. Three replicates with ~350 cells yielded on average 5.3 µg of cDNA, and we observed a high correlation across biological replicates on these dataset (Pearson R=0.90). Thus we aimed for similar cDNA yields by sorting more cells for cell types with a smaller soma (i.e., KCs and PAM cluster DANs). We collected data from ten driver lines for DAN cell types, with 2-4 biological replicates per line. We also examined two classes of KCs and three additional MBON cell types. On average, we collected 2,500 cells for KCs, 546 +/- 60 cells for PAM DANs, and 310 +/- 18 cells for PPL1 DAN and MBON cell types per replicate, by hand or fluorescence activated cell sorting (FACS), yielding 3.53 +/- 0.21 µg of cDNA, 22.3 +/- 0.8 million mapped reads per replicate, and 0.80 +/- 0.02 Pearson R across biological

203 replicates (Figure 3-figure supplement 1; Supplementary File 1).

204 We analyzed these data for different splicing isoforms (see Material and methods). Using
205 DE-seq2 (Love, Huber, & Anders, 2014), we searched for transcripts that were
206 differentially expressed among DAN cell types and, in particular, for those commonly
207 expressed in DAN cell types that showed the valence-inversion phenotype (PPL1-γ1pedc
208 and PAM-γ5), but not in other cell types (Figure 3A,B). Through this analysis, we
209 identified nitric oxide synthase (NOS) as a strong candidate for a cotransmitter. Similar
210 enrichment in PPL1-γ1pedc and PAM-γ5 was found in only five other transcripts, none
211 of which are likely to encode a neurotransmitter: (i) *epac-RG*, a cAMP-activated guanine
212 nucleotide exchange factor. (ii) *br-RO, br-RI,* both transcripts of the zinc finger
213 transcription factor *broad*, (iii) *CG32547-RD*, a G-protein coupled receptor, and (iv)
214 *CG12717-RA*, a SUMO-specific isopeptidase (data reviewed in FlyBase)(Thurmond et
215 al., 2019). In addition to these transcripts that matched our criteria, we found other
216 potential candidates whose expression was not a precise match. We detected a high level
217 of the *DH44* neuropeptide in PPL1-γ1pedc, but not in PAM-γ5. A receptor for DH44,
218 *DH44-R1*, was expressed in PAM-γ4 and/or γ4<γ1γ2 and to lower extent in α/β Kenyon
219 cells, but neither of the two known receptors for DH44 was detected in γ Kenyon cells
220 (Figure 3-figure supplement 2). Transcripts of the neuropeptide gene *Nplp1* were detected
221 in PPL1-γ1pedc and PAM-γ5, but other DANs and MBONs also expressed this gene
222 (Figure 3-figure supplement 2)(Croset, Treiber, & Waddell, 2018). Expression of
223 *Gyc76C*, the receptor for Nplp1, was barely detectable in KCs, DANs, and MBONs.
224 Complete transcript data are presented in Supplementary File 1, and the expression of
225 genes encoding neurotransmitters, neuropeptides and their receptors, as well as

components of gap junctions, is summarized in Figure 3-figure supplement 2. Although we cannot formally rule out a contribution of other genes and pathways, we chose to pursue NOS, as it was the most promising candidate for a cotransmitter that might be responsible for the valence-inversion effect.

Drosophila has only one gene encoding nitric oxide synthase *(Nos)*, but this gene has multiple splicing isoforms (Figure 3C)(Rabinovich, Yaniv, Alyagor, & Schuldiner, 2016; Regulski & Tully, 1995; Stasiv, Regulski, Kuzin, Tully, & Enikolopov, 2001). Only NOS1, the full-length isoform, is functional, while the truncated isoforms can function as a dominant-negative. Thus identifying the expressed splicing isoform of *Nos* was crucial for understanding NOS functions in DANs. NOS1 was the most abundantly expressed isoform as judged by RNA profiling. We confirmed NOS1 expression by combining fluorescent *in situ* hybridization (FISH) and antibody staining. For whole-brain FISH (Long, Colonell, Wong, Singer, & Lionnet, 2017), we used 40 probes against c-terminus exons that are present in NOS1 and NOS4, but not NOS-RK, transcripts (Figures 3C and Figure 3-figure supplement 1 D). PPL1-γ1pedc was labeled with these FISH probes (Figure S3D), confirming expression of NOS1 or NOS4 in these cells. For immunohistochemistry, we used an antibody raised against exon 16 of NOS (Kuntz, Poeck, & Strauss, 2017; Yakubovich, Silva, & O'Farrell, 2010) that is present in NOS1 and NOS-RK, but not in NOS4 (Figure 3C). We validated its specificity by demonstrating a loss of the staining that accompanied RNAi-mediated knockdown of NOS in PPL1-γ1pedc (Figures 3D and Figure 3-figure supplement 1 B)(Ni et al., 2011). In the MB lobes, the γ1pedc and γ5 compartments showed enriched anti-NOS immunoreactivity, as expected from RNA-Seq data. In addition, γ3 and γ4 also showed

significant anti-NOS immunoreactivity (Figures 3E). However, the low NOS transcript levels observed via RNA-Seq in PAM-γ3 and PAM-γ4 are most consistent with anti-NOS immunoreactivity in γ3 and γ4 arising from non-DAN cell types or developmental expression. The cell-type-specific expression and localization of NOS1 in a subset of DANs associated with compartments that display the valence-inversion phenotype prompted us to test the hypothesis that NO plays a direct role in generating the diversity of memory dynamics observed in different compartments.

NOS in dopaminergic neurons contributes to memory formation

We next evaluated the role of NOS in memory formation in the absence of dopamine biosynthesis. If NO is indeed the cotransmitter that supports the valence-inverted memory in TH mutant flies, we would predict that inhibiting NOS should block this effect, and that flies would show no memory. To assess the requirement for NO synthesis, we fed flies the competitive NOS inhibitor L-NNA for one day before training and then measured the memory induced by optogenetic training using PPL1-γ1pedc in a TH mutant background. We found that this treatment reduced valence-inverted memory formation in a dose-dependent manner (Figure 4A). While NOS is broadly expressed in the brain (Kuntz et al., 2017), two lines of evidence suggest that L-NNA fed flies are capable of olfactory learning. First, when we bypassed the TH mutant by by feeding L-DOPA and carbidopa to restore dopamine levels, the L-NNA fed flies showed a normal level of negative-valence odor memory formation in response to pairing an odor with PPL1- γ1pedc activation (Figure 4A). Second, the effect of L-NNA feeding was cell-type specific; memory formed by activation of either PPL1-γ1pedc or PAM-γ5/β'2a was

affected but that formed by activation of PPL1-γ2α'1, was not (Figure 4B). We obtained consistent results in knockdown experiments where we expressed NOS-RNAi in all PPL1 DANs (Figure 4C).

We also examined whether we could transfer this valence-inversion property to another compartment by ectopically expressing NOS. We expressed NOS in PPL1-α3, a compartment where we observed no intrinsic NOS expression, and where extended optogenetic training induces a negative-valence memory (Aso & Rubin, 2016). TH mutant flies formed no odor association with PPL1-α3 activation, but when NOS was ectopically expressed in the α3 compartment, the same training protocol induced a positive-valence memory (Figure 4D and E). In other words, NO was able to form an association of opposite valence to that formed by dopamine. These results demonstrate the functional significance of NOS in DANs, but leave open its mechanism of action.

Soluble guanylate cyclase in Kenyon cells is required to form NO-dependent memories

In the MB, dopamine induces synaptic plasticity by binding to dopamine receptors on the axons of KCs and activating the *rutabaga*-encoded adenylyl cyclase in these cells (Gervasi, Tchenio, & Preat, 2010; Tomchik & Davis, 2009). Does NO released from DANs also act on receptors in the KCs? RNA-seq data revealed expression of the subunits of soluble gyanylate cyclase (sGC), Gycα99B and Gycβ100B, in KCs, DANs, and MBONs (Figure 5A-B). Similar to its mammalian homologs, Drosophila sGC is activated upon binding NO (Morton, Langlais, Stewart, & Vermehren, 2005). Transcripts for other guanylyl cyclases were found at lower levels, if at all (Figure 5A-B;

Supplementary File 1), suggesting that sGC formed by Gycα99B and Gycβ100B is the primary source of cGMP in KCs. Consistent with these transcriptomic data, we observed that a protein trap Gycβ100B-EGFP fusion protein (MI08892; (Venken et al., 2011) was broadly expressed in the MB lobes (Figure 5-figure supplement 1).

We tested the role of Gycβ100B with acute RNAi knockdown in KCs using the MB-switch system (McGuire, Le, Osborn, Matsumoto, & Davis, 2003). This adult-specific knockdown abolished the valence-inverted memory induced by activation of PPL1-γ1pedc in a TH mutant background (Figure 5C). This effect is unlikely to be caused by a developmental defect in KCs, as we could restore normal memory by feeding flies L-DOPA (Figure 5C). Taken together, our data argue strongly that NO functions as cotransmitter that is released by DANs and acts on sGC in postsynaptic KCs to regulate cGMP levels, although our results do not exclude the possibility that NO has other targets.

NO-dependent and dopamine-dependent memories have different kinetics

We next compared the dynamics of memory inducion by NO and dopamine and explored the consequences of their combined action. First, we examined memory acquisition rates when flies were trained by activation of PPL1-γ1pedc (Figure 6A). In wild-type flies, PPL1-γ1pedc activation as brief as 10s can induce significant negative-valence memory. Blocking NOS activity with L-NNA did not affect the memory scores observed shortly after a wide range of training protocols (Figure 6B). In contrast, longer and repetitive training was required to induce robust NO-dependent positive-valence memory in the absence of dopamine (Figure 6A-B).

Riemensperger et al. (2011) reported that dopamine-deficient flies developed weak positive-valence memory after odor-shock conditioning, but this memory was not detectable until two hours after the training. Motivated by this observation, we examined the kinetics of NO-dependent memory formation and the role of NOS in memory retention. When we used a single cycle of training, we found that NO-dependent memory develops slowly over time. Memory scores were not significantly different from zero at 1, 3, 5 min after training, and only became significant after 10 min. Once formed, however, these NO-dependent memories were long lasting and were still more than half maximal after 6 hours (Figure 6C). This result contrasts with the time course of memory formation by PPL1-γ1pedc activation in a wild-type background, where memory is detectable within 1 min after training, but has a half-life of only 2-3 hours (Aso et al., 2012). These observations raised the possibility that NO signaling, with its opposite valence and slower dynamics, might serve to limit memory retention in a wild-type background. Indeed, we found that expression of NOS-RNAi or L-NNA feeding prolonged the retention of memories induced by either optogenetic training with PPL1-γ1pedc or odor-shock conditioning (Figure 6D, Figure 6-figure supplement 1A-B).

Memory persistence is often enhanced by repetitive training. However, PPL1-γ1pedc fails to induce long-lasting memory even after 10x repetitive training at spaced intervals (Aso & Rubin, 2016). In contrast, other DANs from the PPL1 cluster that do not exhibit significant NOS expression, PPL1-α3 or a combination of PPL1-γ2α'1 and PPL1-α'2α2, are able to induce stable memory lasting for four days after 10x spaced training (Aso & Rubin, 2016). Our results strongly suggest that NO signaling is responsible for this difference in memory retention. Spaced training with PPL1-γ1pedc induced memory

lasting 1 day when NOS signaling was compromised, either by knockdown with RNAi (Figure 6E) or inhibition by L-NNA (Figure 6-figure supplement 1C). The valence-inverted memories formed in the γ1pedc compartment following repetitive training in TH mutants also lasted 1 day after training (Figure 6E). Thus, the effects of NOS signaling accumulate slowly, but can be long lasting. These effects are antagonistic to memories formed by dopamine signaling, and serve to sculpt the time course of memory retention. As discussed below, NO-signaling also contributes to other features of memory dynamics.

Nitric oxide enhances fast updating of memory

We designed behavioral experiments to examine memory dynamics when flies that had been previously trained encounter a new experience. We tested three different types of new experience: (1) switching which odor is paired with DAN activation during odor conditioning (reversal conditioning); (2) exposing flies to odors without DAN activation; and (3) activating DANs without odor exposure (Figure 7A). In wild-type flies, odor preference can be altered by a single trial of reversal conditioning with PPL1-γ1pedc activation (Figure 7B, left), whereas this process became slower and required more training when NOS was inhibited (Figure 7B; center), such that switching odor preference required a repetition of reversal conditioning. In TH mutants, NO-dependent memory was also altered by reversal conditioning, but with an even slower time course (Figure 7B; right). The second type of new experience, exposure to odors alone, did not change the existing memory in this assay (Figure 7C). The third type of new experience, DAN activation alone, quickly reduced conditioned odor response in wild-type flies.

Inhibiting NOS slowed this process (Figure 7D; center). NO-dependent memory was also reduced by unpaired activation of DANs, but it took five trials to detect significant reduction (Figure 7D; right). These results suggest that both the slow formation and the persistence of NO-dependent memory facilitate the fast updating of memories stored in NOS-positive MB compartments in response to changing conditions.

Modeling the function of NO and DA in memory dynamics

To understand the interplay between DA and NO dependent plasticity, we fit a minimal model to our data that accounts for the observed effects of these two pathways on formation of odor memories. We then used this model both to infer the parameters of a synaptic plasticity rule consistent with the data as well as to test hypotheses about the mechanisms of DA and NO-mediated synaptic modifications that would be able to generate the memory dynamics we observed. Imaging and physiology experiments have demonstrated that DANs induce intracellular signaling cascades in KCs and bidirectionally modulate the weights of KC-MBON synapses, with the direction of the plasticity determined by whether each KC is active or inactive (Cohn et al., 2015, Gervasi et al., 2010, Hattori et al., 2017, Hige et al., 2015, Berry et al., 2018, Boto et al., 2014, Tomchik and Davis, 2009, Owald et al., 2015, Bouzaiane et al., 2015)(Cassenaer & Laurent, 2012; Okada, Rybak, Manz, & Menzel, 2007). This dependence on presynaptic KC firing ensures the odor-specificity of memories formed following DAN activation. NO-dependent memories, like DA-dependent memories, are odor-specific, suggesting that plasticity induced by NO also depends on KC activity. Based on this observation and

the results of previous studies, we constructed our model by assuming that: (1) both dopamine and NO bidirectionally modulate KC-MBON synapses depending on KC activity, (2) memory decay is due to background levels of DAN activity following conditioning (Placais et al., 2012, Berry et al., 2015, Sitaraman et al., 2015), and (3) the effects of DA and NO occur via independent pathways and can coexist (Figure 6).

Specifically, we denoted the effects of DA and NO-dependent synaptic plasticity at time *t* by two quantities, *D(t)* and *N(t)*, that lie between 0 and 1. We assumed that coincident KC-DAN activation increases *D* and *N* with a timescale of 30 s and 10 min, respectively, to account for the slower induction of NO-mediated effects (Fig. 8A,B). Based on previous observations in TH wild type flies that pairing of activation of the PPL1- γ1pedc DAN with odor induces synaptic depression between odor activated KCs and MBON-γ1pedc>α/β (Hige et al., 2015), we assumed that the effect of an increase in *D* is a reduction in the weight of the corresponding KC-MBON synapse (Fig. 8B, left). As the activity of this MBON promotes approach behavior (Aso et al., 2014b, Owald et al., 2015), its reduced response to the conditioned odor after DA-dependent synaptic depression results in avoidance during subsequent odor presentations. In the TH-null background, in contrast, we have shown that PPL1-γ1pedc activation leads to a positive-valence memory (Figure 2). This is most readily explained in our model by assuming that, in such flies, NO induces potentiation of synapses between odor-activated KCs and MBONs (Fig. 8B, right). Thus, in the model, the effect of an increase in *N* is an increase in synaptic weight, opposite to the effect of *D*. Finally, based on observations that activation of DANs alone can reverse synaptic depression induced by KC-DAN pairing (Cohn et al., 2015, Hattori et al., 2017, Berry et al., 2018), we assumed that DAN

activation in the absence of KC activity causes a reduction in D and N, recovering the synapse to its baseline weight.

We fit the model by assuming that the performance index (PI) is determined by the odor-evoked activation of the MBON and then determining the parameters that best match the behavioral data reported in Figure 6B-D. We used data that isolates the effects of DA and NO dependent plasticity mechanisms to fit the parameters for the two pathways separately (see Methods). In the resulting model, NO-dependent plasticity develops more gradually and requires more KC-DAN pairings to produce a memory of equal magnitude, compared to DA-dependent plasticity (Fig. 8C).

We next asked how these plasticity mechanisms interact to determine effective KC-to-MBON synaptic weights when both DA and NO pathways are active. The synaptic weight is a function of both DA and NO-mediated effects, $w = f(D,N)$. One possibility for the function f is a difference between terms corresponding to DA-dependent depression and NO-dependent facilitation; that is, $w \propto N - D$. When we fit a model with this functional form to our data, we found that it incorrectly predicts a reduction in memory strength after repeated pairings, because of the slower accumulation of NO-dependent facilitation after DA-dependent potentiation has saturated (Figure 8D, gray curve). Another possibility for f is a multiplicative form, e.g. $w \propto (1 - D) \times (1 + N)$. While we cannot unambiguously determine the identity of the biophysical parameters underlying DA and NO-mediated effects, such a form would arise naturally if the two pathways modulated parameters such as quantal size and the probability of synaptic vesicle release from KCs. We found that the multiplicative model provides a good match to our data

(Figure 8C, blue curve). In this model, strong DA-dependent depression (i.e. *D* close to 1) leads to a small synaptic weight even in the presence of NO-dependent facilitation.

We further tested our model by investigating its behavior in other paradigms. Assuming that spontaneous activity in DANs leads to memory decay (Placais et al., 2012, Berry et al., 2015, Sitaraman et al., 2015) accounted for the NO-dependent reduction in memory lifetime that we observed (Figure 8E). Fitting the magnitudes of DA-dependent facilitation and NO-dependent depression in the absence of KC activity using the data of Figure 7D also predicted the dynamics of reversal learning and its facilitation by NO with no additional free parameters (Figure 8F). In total, modeling a multiplicative interaction between DA- and NO-dependent plasticity accounts for the immediate effects of these pathways on odor memories that we observed experimentally. A notable exception is that this model cannot account for the enhanced persistence of memories after 10x training for DA or NO-null conditions (Figure 6E), suggesting a recruitment of additional consolidation mechanisms after spaced conditioning, as previously proposed (Pagani et al., 2009, Tully et al., 1994, Pai et al., 2013, Scheunemann et al., 2018, Cervantes-Sandoval et al., 2013, Miyashita et al., 2018, Huang et al., 2012, Akalal et al., 2011).

Discussion

Evidence from a wide range of organisms establishes that dopaminergic neurons often release a second neurotransmitter, but the role of such cotransmitters in diversifying neuronal signaling is much less clear. In rodents, subsets of dopaminergic neurons co-release glutamate or GABA (Maher & Westbrook, 2008; Stuber et al., 2010; Sulzer et al., 1998; Tecuapetla et al., 2010; Tritsch et al., 2012). In mice and Drosophila, single-cell expression profiling reveals expression of diverse neuropeptides in dopaminergic neurons (Croset et al., 2018; Poulin et al., 2014). EM connectome studies of the mushroom body in adult and larval Drosophila reveal the co-existence of small-clear-core and large-dense-core synaptic vesicles in individual terminals of dopaminergic neurons (Eichler et al., 2017; Takemura et al., 2017); moreover, the size of the observed large-dense-core vesicles differs between DAN cell types (Takemura et al., 2017).

We found that NOS, the enzyme that synthesizes NO, was located in the terminals of a subset of DAN cell types. NOS catalyzes the production of nitric oxide (NO) from L-arginine. Drosophila NOS is regulated by Ca^{2+}/calmodulin (Regulski & Tully, 1995), as is the neuronal isoform of NOS in the mammalian brain (Abu-Soud & Stuehr, 1993), raising the possibility that NO synthesis might be activity dependent. Furthermore, the localization of the NOS1 protein in the axonal terminals of DANs (Figure 3D) is consistent with NO serving as a cotransmitter. Our conclusion that NO acts as a neurotransmitter is supported by the observation that NO signaling requires the presence of a putative receptor, soluble guanylate cyclase, in the postsynaptic Kenyon cells. This role contrasts with the proposed cell-autonomous action of NOS in the ellipsoid body, in

466 which NO appears to target proteins within the NOS-expressing ring neurons themselves,
467 rather than conveying a signal to neighboring cells (Kuntz et al., 2017).

468 The valence-inversion phenotype we observed when PPL1-γ1pedc was
469 optogenetically activated in a dopamine-deficient background can be most easily
470 explained if NO induces synaptic potentiation between odor-activated KCs and their
471 target MBONs. Our modeling work is consistent with this idea, but testing this idea and
472 other possible mechanisms for NO action will require physiological experiments.
473

474 **Antagonistic functions of dopamine and nitric oxide**

475 During olfactory learning, the concentration of Ca^{2+} in KC axons represents olfactory
476 information. The coincidence of a Ca^{2+} rise in spiking KCs and activation of the G-
477 protein-coupled Dop1R1 dopamine receptor increases adenylyl cyclase activity (Abrams,
478 Yovell, Onyike, Cohen, & Jarrard, 1998; Boto, Louis, Jindachomthong, Jalink, &
479 Tomchik, 2014; Byrne et al., 1991; Kim, Lee, & Han, 2007; McGuire et al., 2003;
480 Tomchik & Davis, 2009). The resultant cAMP in turn activates protein kinase A (Gervasi
481 et al., 2010; Skoulakis, Kalderon, & Davis, 1993), a signaling cascade that is important
482 for synaptic plasticity and memory formation throughout the animal phyla (e.g. Davis,
483 Cherry, Dauwalder, Han, & Skoulakis, 1995). In contrast, when DANs are activated
484 without KC activity, and thus during low intracellular Ca^{2+} in the KCs, molecular
485 pathways involving the Dop1R2 receptor, Rac1 and Scribble facilitate decay of memory
486 (Berry, Cervantes-Sandoval, Nicholas, & Davis, 2012; Cervantes-Sandoval, Chakraborty,
487 MacMullen, & Davis, 2016; Kim et al., 2007; Shuai et al., 2010).

We found that NOS in PPL1-γ1pedc shortens memory retention, while facilitating fast updating of memories in response to new experiences. These observations could be interpreted as indicating that NO regulates forgetting. However, it is an open question whether the signaling pathways for forgetting, which presumably induce recovery from synaptic depression (Berry et al., 2018; Cohn et al., 2015), are related to signaling cascades downstream of NO and guanylate cyclase, which appear to be able to induce memory without prior induction of synaptic depression by dopamine. Lack of detectable 1-day memory formation after spaced training with PPL1-γ1pedc can be viewed as a balance between two distinct, parallel biochemical signals, one induced by dopamine and the other by NO, rather than the loss of information (that is, forgetting). Confirming this interpretation will require better understanding of the signaling pathways downstream of dopamine and NO. The search for such pathways will be informed by the prediction from our modeling that dopamine and NO may alter two independent parameters that define synaptic weights with a multiplicative interaction.

In the vertebrate cerebellum, which has many architectural similarities to the MB (Farris, 2011; Marr, 1969; Medina, Repa, Mauk, & LeDoux, 2002), long-term-depression at parallel fiber-Purkinje cell synapses (equivalent to KC-MBON synapses) induced by climbing fibers (equivalent to DANs) can coexist with long-term-potentiation by NO (Bredt, Hwang, & Snyder, 1990; Lev-Ram, Wong, Storm, & Tsien, 2002; Shibuki & Okada, 1991). In this case, the unaltered net synaptic weight results from a balance between coexisting LTD and LTP rather than recovery from LTD. This balance was suggested to play an important role in preventing memory saturation in the cerebellum and allowing reversal of motor learning. In the *Drosophila* MB, we observed a similar

facilitation of reversal learning by NO (Figure 7B). The antagonistic roles of NO and synaptic depression may be a yet another common feature of the mushroom body and the cerebellum.

Distinct dynamics of dopamine and nitric oxide

Opposing cotransmitters have been observed widely in both invertebrate and vertebrate neurons (Nusbaum, Blitz, & Marder, 2017). A common feature in these cases is that the transmitters have distinct time courses of action. For instance, hypothalamic hypocretin-dynorphin neurons that are critical for sleep and arousal synthesize excitatory hypocretin and inhibitory dynorphin. When they are released together repeatedly, the distinct kinetics of their receptors result in an initial outward current, then little current, and then an inward current in the postsynaptic cells (Y. Li & van den Pol, 2006). In line with these observations, we found that dopamine and NO show distinct temporal dynamics: NO-dependent memory requires repetitive training and takes longer to develop than dopamine-dependent memory. What molecular mechanisms underlie these differences? Activation of NOS may require stronger or more prolonged DAN activation than does dopamine release. Alternatively, efficient induction of the signaling cascade in the postsynaptic KCs might require repetitive waves of NO input. Direct measurements of release of dopamine and NO, and downstream signaling events by novel sensors will be needed to address these open questions (Chen, Saulnier, Yellen, & Sabatini, 2014; Eroglu et al., 2016; Patriarchi et al., 2018; Sun et al., 2018; Tang & Yasuda, 2017).

Toward subcellular functional mapping of memory genes

Decades of behavioral genetic studies have identified more than one hundred genes underlying olfactory conditioning in *Drosophila* (Keene & Waddell, 2007; McGuire, Deshazer, & Davis, 2005; Thurmond et al., 2019; Walkinshaw et al., 2015). Mutant and targeted rescue studies have been used to map the function of many memory-related genes encoding synaptic or intracellular signaling proteins (for example, rutabaga, DopR1/dumb, DopR2/DAMB, PKA-C1/DC0, Synapsin, Bruchpilot, Orb2 and Rac1) to specific subsets of Kenyon cells (Akalal et al., 2006; Berry et al., 2012; A. L. Blum, W. H. Li, M. Cressy, & J. Dubnau, 2009; Gervasi et al., 2010; Han, Millar, Grotewiel, & Davis, 1996; Kim et al., 2007; Knapek, Sigrist, & Tanimoto, 2011; Kruttner et al., 2015; McGuire et al., 2003; Niewalda et al., 2015; Pavot, Carbognin, & Martin, 2015; Qin et al., 2012; Shuai et al., 2010; Skoulakis et al., 1993; Trannoy et al., 2011; Vanover et al., 2018; Zars et al., 2000). However, it is largely unknown if these proteins physically colocalize at the same KC synapses to form intracellular signaling cascades. Some of these proteins might preferentially localize to specific MB compartments. Alternatively, they may distribute uniformly along the axon of Kenyon cells, but be activated in only specific compartments. Our identification of cell-type-specific cotransmitters in DANs enabled us to begin to explore this question.

We used optogenetic activation of specific DANs to induce memory in specific MB compartments, while manipulating genes in specific types of Kenyon cells. This approach allowed us to map and characterize the function of memory-related genes at a subcellular level. For example, the Gycbeta100B gene, which encodes a subunit of sGC, has been identified as “memory suppressor gene” that enhances memory formation when pan-neuronally knocked down (Walkinshaw et al., 2015), but the site of its action was

unknown. Gycbeta100B appears to be broadly dispersed throughout KC axons, based on the observed distribution of a Gycbeta100B-EGFP fusion protein (Figure 5 -figure supplement 1). Our experiments ectopically expressing NOS in PPL1-α3 DANs that do not normally signal with NO is most easily explained if sGC is available for activation in all MB compartments (Figure 4D-E).

What are the molecular pathways downstream to cGMP? How do dopamine and NO signaling pathways interact in regulation of KC synapses? Previous studies and RNA-Seq data suggest several points of possible crosstalk. In cultured KCs from cricket brains, cGMP-dependent protein kinase (PKG) mediates NO-induced augmentation of a Ca^{2+} channel current (Kosakai, Tsujiuchi, & Yoshino, 2015). However, we failed to detect expression of either of the genes encoding Drosophila PKGs (foraging and Pkg21D) in KCs in our RNA-Seq studies (Figure 3-figure supplement 2). On the other hand, cyclic nucleotide-gated channels and the cGMP-specific phosphodiesterase Pde9 are expressed in KCs. Biochemical studies have shown that the activity of sGC is calcium dependent and that PKA can enhance the NO-induced activity of sGC by phosphorylating sGC; sGC isolated from flies mutant for adenylate cyclase, *rutabaga*, show lower activity than sGC from wild-type brains (Morton et al., 2005; Shah & Hyde, 1995), suggesting crosstalk between the cAMP and cGMP pathways.

The benefits of parallel memory units with heterogeneous dynamics

All memory systems must contend with a tension between the strength and longevity of the memories they form. The formation of a strong immediate memory interferes with and shortens the lifetimes of previously formed memories, and reducing this interference

582 requires a reduction in initial memory strength that can only be overcome through
583 repeated exposure (Amit & Fusi 1994). Theoretical studies have argued that this tension
584 can be resolved by memory systems that exhibit a heterogeneity of timescales, balancing
585 the need for both fast, labile memory and slow consolidation of reliable memories (Fusi,
586 Drew & Abbott 2005, Lahiri & Ganguli 2013, Benna & Fusi 2016). The mechanisms
587 responsible for this heterogeneity, and whether they arise from complex signaling within
588 synapses themselves (Benna & Fusi 2016), heterogeneity across brain areas (Roxin &
589 Fusi 2013), or both, have not been identified.
590
591 We found that NO acts antagonistically to dopamine and reduces memory retention
592 (Figure 6) while facilitating the rapid updating of memory following a new experience
593 (Figure 7). Viewed in isolation, the NO-dependent reduction in memory retention within
594 a single compartment may seem disadvantageous, but in the presence of parallel learning
595 pathways, this shortened retention may represent a key mechanism for the generation of
596 multiple memory timescales that are crucial for effective learning. During shock
597 conditioning, for example, multiple DANs respond to the aversive stimulus, including
598 PPL1-γ1pedc, PPL1-γ2α'1, PPL1-α3 (Mao and Davis, 2009, Riemensperger et al., 2005).
599 We have shown that optogenetic activation of these DAN cell types individually induces
600 negative-valence olfactory memory with distinct learning rates (Aso & Rubin, 2016). The
601 NOS-expressing PPL1-γ1pedc induces memory with the fastest learning rate in a wild-
602 type background, and we show here that it induces an NO-dependent memory trace when
603 dopamine synthesis is blocked, with a much slower learning rate and opposite valence.
604 Robust and stable NO-dependent effects were only observed when training was repeated

10 times (Figure 6E). Under such repeated training, compartments with slower learning rates, such as α3, form memory traces in parallel to γ1pedc (Pai et al., 2013; Sejourne et al., 2011; Wu et al., 2017). Thus, flies may benefit from the fast and labile memory formed in γ1pedc (Figure 7) without suffering the potential disadvantages of shortened memory retention, as long-term memories are formed in parallel in other compartments. The Drosophila MB provides a tractable experimental system to study the mechanisms and benefits of diversifying learning rate, retention, and flexibility in parallel memory units, as well as exploring how the outputs from such units are integrated to drive behavior.

Acknowledgements

We thank Jui-Chun Kao, and the Janelia Fly Facility for help with fly husbandry. We thank Eizaburo Doi, Joshua Dudman, Yichun Shuai, Mehrab Modi, Karen Hibbard Gowan Tervo, Adam Hantman, Daisuke Hattori, Larry Abbott, Vanessa Ruta, Stott Waddell, Hiromu Tanimoto, Toshihide Hige, Brett Mensh and Glenn Turner for stimulating discussions and for comments on earlier drafts of the manuscript. Nikita Yakubovich and Patrick O'Farrell shared anti-NOS 16 serum pET28a-dNOS exon 16 plasmid. Phil Borden, Gaby Paez, Silvia Sanchez Martinez, Ariana Tkachuk, Tim Brown, Yan Zhang, Lauren Porter, Jonathan Marvin, and Loren Looger provided guidance on affinity purification of the anti-NOS antibody. Burkhard Poeck and Roland Strauß shared confocal images of fly brains stained with anti-NOS. Rebecca Vorimo, Allison Sowell, Kari Close, Project Technical Resources, and the FlyLight Project Team at Janelia Research Campus provided brain dissection and histological preparation. The laboratory of J.H. was supported by NIH R01 GM GM84128.

Author Contributions

Y.A. and G.M.R. conceived and designed the study. Y.A. acquired the behavioral and anatomical data. R.R. and A.L. performed the RNA-Seq data acquisition and analysis. X.L. performed RNA FISH experiments. A.L.-K. performed computational modeling. K.C. and J.H. provided key reagents. B. S., T.N. and C.C. provided technical assistance. Y.A, A.L.-K. and G.M.R. wrote the article.

638

639 **Declaration of Interests**

640 The authors declare no competing interests.

641

642 # Materials and methods

643 ## KEY RESOURCES TABLE

REAGENT or RESOURCE	SOURCE	IDENTIFIER
Antibodies		
Mouse monoclonal anti-Brp	*Developmental Studies Hybridoma Bank*	nc82
Mouse monoclonal anti-TH	Millipore-Sigma	MAB318
Rabbit polyclonal anti-NOS exon 16	Yakubovich et al., 2010 PMID: 20178753 This paper	N.A.
Chicken polyclonal anti-GFP	abcam	ab13970
Goat anti-Rabbit IgG (H+L) Highly Cross-Adsorbed Secondary Antibody, Alexa Fluor 568	Invitrogen	A-11036
Goat anti-Chicken IgY (H+L) Secondary Antibody, Alexa Fluor 488	Invitrogen	A-11039
Anti-Mouse IgG (H&L) (Goat), ATTO 647N conjugated	ROCKLAND antibodies & assays	610-156-121
Bacterial and Virus Strains		
T7 Express lysY/lq	New England BioLabs	C3013
Chemicals, Peptides, and Recombinant Proteins		
S-(−)-Carbidopa	Millipore-Sigma	C1335
L-DOPA	Millipore-Sigma	D9628
L-NNA (Nu-nitro-L-arginin)	Millipore-Sigma	N5501
Schneider's Drosophila Medium	Thermo Fisher Scientific	21720024
RU-486	Millipore-Sigma	475838
Cy®5 Mono	GE Healthcare	PA25001
Cy®3 Mono	GE Healthcare	PA23001
RNase-free water: Molecular Biology Grade Water	Corning	46-000-CM
RNase-free 1x PBS	Fisher	BP2438-4
CH3COOH: Acetic Acid	Fisher	A38S-500
NaBH4: Sodium borohydride, 99%, VenPure™ SF powder	Acros Organics	AC448481000
20xSSC	Fisher	AM9763
Hi-Di formamide	Applied Biosystems	4440753
50x Denhardt's solution	Alfa Aesar	AAJ63135AD
tRNA: baker's yeast	Roche	10109495001
UltraPure™ Salmon Sperm DNA Solution	Thermofisher	15632011
10% SDS	Corning	46-040-CI
Formamide (Deionized)	Ambion	AM9342
Liberase DH	Roche	5401054001
Critical Commercial Assays		
PicoPure RNA Isolation Kit	Life Technologies	NEG772014MC
AminoLink Immobilization Kit	Thermo Scientific	#44890
Experimental Models: Organisms/Strains		
D. melanogaster: *20xUAS-CsChrimson-mVenus attP18*	Klapoetke et al., 2014 PMID: 24509633	N.A.
D. melanogaster: *ple2, DTHFS$^{+/-}$ BAC in attP2*	Cichewicz et al., 2017 PMID: 27762066	N.A.

D. melanogaster: *UAS-DTH*	Cichewicz et al., 2017 PMID: 27762066	N.A.
D. melanogaster: *TH-ZpGAL4DBD in VK00027*	Aso et al., 2014a PMID: 25535793	N.A.
D. melanogaster: *DDC-ZpGAL4DBD in VK00027*	Aso et al., 2014a PMID: 25535793	N.A.
D. melanogaster: *R52H03-p65ADZp attP40*	Aso et al., 2014a PMID: 25535793	N.A.
D. melanogaster: *R58E02-p65ADZp attP40*	Aso et al., 2014a PMID: 25535793	N.A.
D. melanogaster: *Gr66a-LexA*	Aso et al., 2014a PMID: 25535793	N.A.
D. melanogaster: *13xLexAop2-CsChrimson-mVenus attP18*	Klapoetke et al., 2014 PMID: 24509633	N.A.
D. melanogaster: *pBPp65ADZpUw attP40*	Seeds et al., 2014 PMID: 25139955	N.A.
D. melanogaster: *VT045661-LexAp65 in JK22C*	Aso et al., 2016 PMID: 27441388	N.A.
D. melanogaster: *R73F07-p65ADZp attP40*	Aso et al., 2014a PMID: 25535793	N.A.
D. melanogaster: *R72B05-p65ADZp attP40*	Aso et al., 2014a PMID: 25535793	N.A.
D. melanogaster: *R24E12-p65ADZp attP40*	Aso et al., 2014a PMID: 25535793	N.A.
D. melanogaster. UAS-NOS-shRNA strain#1 y[1] sc[*] v[1]; P{y[+t7.7] v[+t1.8]=TRiP.HMC03076}attP2 (VALIUM20 vector; TCGGAGCAATATGCGAAGCAA)	Bloomington Drosophila Stock Center	50675
D. melanogaster. UAS-NOS-shRNA strain#2 SH09526.N in attP40 (VALIUM20 vector; ACCACTGGACATTATCAGCTA)	this study; Parkins et al., 2015 PMID: 26320097	N.A.
D. melanogaster. RNAi background for attP2	Bloomington Drosophila Stock Center	36303
D. melanogaster. RNAi background for attP40	Bloomington Drosophila Stock Center	36304
D. melanogaster. UAS-NOS	Bloomington Drosophila Stock Center	56823
D. melanogaster. MB-Switch	Mao et al., 2004 PMID: 14684832	N.A.
D. melanogaster: Gycbeta100B-RNAi w; P{y[+t7.7] v[+t1.8]=TRiP.HMJ22589}attP40	Bloomington Drosophila Stock Center	N.A.
D. melanogaster: Gycbeta100B[MI08892-GFSTF.2]	Bloomington Drosophila Stock Center Nagarkar-Jaiswal et al., 2015, PMID: 25824290	60565
D. melanogaster: *MB320C-split-GAL4*	Aso et al., 2014a PMID: 25535793	N.A.
D. melanogaster: UAS-7xHalo7::CAAX in attP40	Bloomington Drosophila Stock Center Sutcliffe et al., 2017 PMID: 28209589	67621
Oligonucleotides		
NOS FISH prob#01_CGCGCCGCAAGCTCAAGA	Biosearch Technologies	N.A.
NOS FISH prob#02_CCTAGCGCGACTTTTGAC	Biosearch Technologies	N.A.
NOS FISH prob#03_TCCTGGTGTGTCTCTATT	Biosearch Technologies	N.A.
NOS FISH prob#04_AACAGTCACTTCACTGGC	Biosearch Technologies	N.A.
NOS FISH prob#05_TCTTCTCACCTCTCTTTA	Biosearch Technologies	N.A.
NOS FISH prob#06_ACTTCGTTAACTCACGCC	Biosearch Technologies	N.A.

NOS FISH prob#07_CTCGGCGTCTTTCAAACG	Biosearch Technologies	N.A.
NOS FISH prob#08_ACCTCCCATTTAACAGGT	Biosearch Technologies	N.A.
NOS FISH prob#09_ACCAAGTGGACAACCGAC	Biosearch Technologies	N.A.
NOS FISH prob#10_TTGCTCCGTTTGTTAGTC	Biosearch Technologies	N.A.
NOS FISH prob#11_CTCGACGAGGTGCAAGGG	Biosearch Technologies	N.A.
NOS FISH prob#12_CTGTTCTACAGCGTCGTA	Biosearch Technologies	N.A.
NOS FISH prob#13_TTGGACGCTAAGCACTGG	Biosearch Technologies	N.A.
NOS FISH prob#14_CGTGTCTGTGTCGTTGTT	Biosearch Technologies	N.A.
NOS FISH prob#15_GTTTTGAGTTCGTTGCGG	Biosearch Technologies	N.A.
NOS FISH prob#16_CAACTTACCGTTACCCGA	Biosearch Technologies	N.A.
NOS FISH prob#17_ACTCGCCGTTAGGTTTAC	Biosearch Technologies	N.A.
NOS FISH prob#18_GCCACTGAGGAGCGGGTC	Biosearch Technologies	N.A.
NOS FISH prob#19_TACTTCACCTGGTAGGCC	Biosearch Technologies	N.A.
NOS FISH prob#20_GTGTTCCTCGAGTTCGTC	Biosearch Technologies	N.A.
NOS FISH prob#21_CCTCCGAACGGTAGAAGT	Biosearch Technologies	N.A.
NOS FISH prob#22_CGGTAACTCCGTGGTGTT	Biosearch Technologies	N.A.
NOS FISH prob#23_CGCGGTCATAGAGGTGTC	Biosearch Technologies	N.A.
NOS FISH prob#24_AGCGGAGGTTAGGCGCTT	Biosearch Technologies	N.A.
NOS FISH prob#25_CGTGGTTGTGGTCGTAGC	Biosearch Technologies	N.A.
NOS FISH prob#26_CAGCTTGACCTACCGTCA	Biosearch Technologies	N.A.
NOS FISH prob#27_ACCGCAACCGCAACCAGT	Biosearch Technologies	N.A.
NOS FISH prob#28_CACGCCCAACAGGAGGGA	Biosearch Technologies	N.A.
NOS FISH prob#29_GACGTGACGCAGGCCTTT	Biosearch Technologies	N.A.
NOS FISH prob#30_CAAGCGCCCTTGATAGCG	Biosearch Technologies	N.A.
NOS FISH prob#31_AGCGGCTTTTTGGTTGTC	Biosearch Technologies	N.A.
NOS FISH prob#32_CGGGTCTTTCTACAGTGT	Biosearch Technologies	N.A.
NOS FISH prob#33_TAATAGCCAGCGCACGGC	Biosearch Technologies	N.A.
NOS FISH prob#34_AATACGTGGACCTGCTGC	Biosearch Technologies	N.A.
NOS FISH prob#35_GTCAGACGACTACGCGTT	Biosearch Technologies	N.A.
NOS FISH prob#36_CTGACTTCTTGTAGCTCC	Biosearch Technologies	N.A.
NOS FISH prob#37_CTCCAGATGCTGTGCGAC	Biosearch Technologies	N.A.
NOS FISH prob#38_GACGTTCCCAGCGCTCTA	Biosearch Technologies	N.A.
NOS FISH prob#39_AAAGGACGAGCTTCCGGT	Biosearch Technologies	N.A.
NOS FISH prob#40_ACATGCTCGTCGTAATAC	Biosearch Technologies	N.A.
Recombinant DNA		
pET28a-dNOS exon 16	Yakubovich et al., 2010 PMID: 20178753	N.A.
pRSET-dNOS exon 16	This paper	N.A.
Software and Algorithms		
DE-seq2	Love et al., 2014 PMID: 25516281	N.A.

Fiji	Schindelin et al., 2012 PMID: 22743772	N.A.
MATLAB	MathWorks	N.A.
Prism	GraphPad	N.A.

644

645 **Flies**

646 Drosophila strains used in this study are listed in the KEY RESOURCES TABLE. Crosses
647 were kept on standard cornmeal food supplemented with retinal (0.2 mM all-trans-retinal
648 prior to eclosion and then 0.4 mM) at 21°C at 60% relative humidity in the dark. Female
649 flies were sorted on cold plates at least 1 d prior to the experiments, and 4-10 d old flies
650 were used for experiments. Additional drugs were administered by feeding with retinal
651 containing fly food mixed with drugs. The L-DOPA (D9628, Sigma) or L-NNA were mixed
652 directly into melted fly food at final concentrations of 1 mg/ml or 1-100mM, respectively.
653 S-(−)-Carbidopa (C1335, Sigma) was dissolved in 1 ml of water at 10x the final
654 concentration and mixed with 9 ml of melted fly food.

655 **Olfactory learning assay**

656 Groups of approximately 20 female flies, 4–10 d post-eclosion, were trained and tested at
657 25°C at 50% relative humidity in the fully automated olfactory arena for optogenetics
658 experiments (Aso & Rubin, 2016; Pettersson, 1970; Vet, Vanlenteren, Heymans, & Meelis,
659 1983). The odors were diluted in paraffin oil (Sigma–Aldrich): 3-octanol (OCT; 1:1000;
660 Merck) and 4-methylcyclohexanol (MCH; 1:750; Sigma–Aldrich). Videography was
661 performed at 30 frames per second and analyzed using Fiji (Schindelin et al., 2012).
662 Statistical comparisons were performed (Prism; Graphpad Inc, La Jolla, CA 92037) using
663 the Kruskal Wallis test followed by Dunn's post-test for multiple comparison, except those
664 in Figure 6 which used Wilcoxon signed-rank test with Bonferroni correction to compare
665 from zero.

666

667 **Immunohistochemistry**

668 Dissection and immunohistochemistry of fly brains were carried out as previously described
669 with minor modifications (Jenett et al., 2012) using the antibodies listed in KEY
670 RESOURCES TABLE. Brains and VNCs of 3- to 10-day old female flies were dissected in
671 Schneider's insect medium and fixed in 2% paraformaldehyde in Schneider's medium for 55
672 min at room temperature (RT). After washing in PBT (0.5% Triton X-100 in PBS), tissues
673 were blocked in 5% normal goat serum (or normal donkey serum, depending on the
674 secondary antibody) for 90 min. Subsequently, tissues were incubated in primary antibodies
675 diluted in 5% serum in PBT for 2–4 days on a nutator at 4°C, washed four times in PBT for
676 15 min or longer, then incubated in secondary antibodies diluted in 5% serum in PBT for 2–
677 4 days on a Nutator at 4°C. Tissues were washed thoroughly in PBT four times for 15 min
678 or longer and mounted on glass slides with DPX.

679 For immunolabeling of NOS, the serum against NOS exon 16 was obtained from N.
680 Yakuobovich and P. H. O'Farrell (Yakubovich et al., 2010), and then affinity purified as
681 described below. In order to minimize non-specific signals, we absorbed 200 µL of anti-
682 NOS antibody (1:1000) for one day with 30 fly brains in which NOS was knocked down
683 panneuronally using elav-GAL4 and NOS-RNAi strain#1 (TRiP.HMC03076), and the
684 supernatant was used for subsequent immunohistochemistry.

685

686 **Purification of dNOS proteins and antibody**

687 The pRSET-dNOS exon 16 construct, containing an N-terminal His tag and T7 gene 10
688 leader RBS site, was assembled as follows. The NEBuilder Assembly tool was used to

689 design primers for the NEBuilder HiFi DNA assembly (New England Biolabs # E2621S)
690 of dNOS exon 16 as contained in pET28a-dNOS exon 16 (gift of Nikita Yakubovich, O-
691 Farrell lab, UCSF) into the backbone vector pRSET (gift of Ariana Tkachuk, Janelia)
692 which was digested with BamHI/EcoRI. The assembled product, pRSET-dNOS exon 16,
693 was first transformed into NEB 5-alpha competent cells (New England Biolabs
694 #E2621S) and plated on LB plus ampicillin (60 µl/ml).

695 For protein purification, pRSET-dNOS exon 16 DNA was then transformed into
696 T7 Express lysY/lq *E.coli* protein expression cells (New England Biolabs #C3013) and
697 plated on LB plus ampicillin (60 µl/ml). For large-scale growth, 500 ml of Miller's LB
698 plus ampicillin (60 µl/ml) was inoculated from 5 ml of a starter culture and grown for
699 ~3 hrs (~O.D. 0.5-0.7) at 37 °C and then induced by adding 0.5 mM IPTG. The culture
700 was allowed to grow at 18-20 °C overnight before spinning down and freezing the
701 recovered pellets which were divided in two 250 ml bottles.

702 To resuspend the thawed pellets (frozen overnight), 10-12 ml of the nonionic detergent-
703 based lysis reagent B-PER (Thermo Scientific #78266) in phosphate buffer containing
704 1mg/ml of lysozyme (Thermo Scientific #89833), nuclease (0.1 µl/ml, Thermo Scientific
705 # 88701), and 1X HALT protease inhibitors (Thermo Scientific #1861279). The
706 suspension, divided into two 50 ml conical tubes, was gently shaken for 15-20 min at 30
707 °C before spinning down at 8,000 x g for 15 mins at 4 °C. We found that that the majority
708 of the dNOS exon 16 protein was in inclusion bodies and therefore we carried out
709 purification starting with the pellet .

710 Each pellet was resuspended in ~10 ml B-PER containing 200 µg/ml lysozyme.
711 The suspension was then mixed with 100 ml of a wash buffer containing 1:10 B-PER in

ice cold 1xPBS (diluted from 10X PBS stock, Fisher Scientific #BP3994) by pipetting the mixture up and down and gentle agitation. The mixture was spun down at 15,000 rpm for 15 min at 4 °C. The pellet was similarly washed four more times. The washed pellet was either stored at -20 °C overnight or resuspended in 7-12 ml of inclusion body solubilization reagent (Thermo Scientific #78115). The protein suspension was shaken for 30-40 min at 20 °C and then ultracentrifuged at 35,000 x g for 20-30 min at 4 °C.

For affinitiy purification of anti-dNOS antibody, the supernatant fraction was concentrated using 50 ml conical tubes Vivaspin 20, 10,000 MWCO concentrators (Sartorius # VS2002) and then dialyzed in 3-12 ml dialysis cassettes 10,000 MWCO (Thermo Scientific #66810) against 1L of 4M guanidine HCL (diluted from 6M stock, Sigma #SRE0066) in 1X PBS pH 8.0 for ~ 6 hours at 4 °C. The medium was further diluted to 2M guanidine HCL and the protein continued to dialyze overnight. Affinity purification of the protein-antibody complex was performed using the AminoLink Immobilization Kit (Thermo Scientific #44890). Approximately 6 mg of soluble dNOS exon 16 protein in 2M guanidine in 1X PBS was bound to the agarose beads in the column as antigen, and 1.9 ml of crude rabbit anti sera to dNOS exon 16 (gift of Nikita Yakubovich of Patrick O-Farrell's lab) was run through the column. The purified dNOS exon 16 rabbit anti-antibody fractions were eluted with IgG Elution buffer (Thermo Scientific # 21004) and then concentrated with Vivaspin 20 tube concentrators before dialyzed in 1XPBS at 4 °C for 2.5 days with one change of fresh 1X PBS.

FISH

735 The fluorescence in situ hybridization (FISH) probe libraries were designed based on
736 transcript sequences and were purchased from Biosearch Technologies. The FISH protocol
737 and dye labeling procedures were described previously (Long et al., 2017). FISH probes for
738 detecting tyrosine hydroxylase transcripts were described (Meissner et al., 2019). FISH
739 probes for NOS are listed in KEY RESOURCES TABLE. Each probe contains a 3'-end
740 amine-modified nucleotide that allows directly couple to an NHS-ester Cy3 dye (GE
741 Healthcare, PA23001) according to the manufacturer's instructions. The brains of 3-5 d old
742 adult flies were dissected in 1xPBS and fixed in 2% paraformaldehyde diluted PBS at room
743 temperature for 55 min. Brain tissues were washed in 0.5% PBT, dehydrated, and stored in
744 100% ethanol at 4°C. After exposure to 5% acetic acid at 4 °C for 5 min, the tissues were
745 fixed in 2% paraformaldehyde in 1xPBS for 55 min at 25 °C. The tissues were then washed
746 in 1× PBS with 1% of $NaBH_4$ at 4 °C for 30 min. Following a 2 h incubation in
747 prehybridization buffer (15% formamide, 2× SSC, 0.1% Triton X-100) at 50 °C, the brains
748 were introduced to hybridization buffer (10% formamide, 2x SSC, 5x Denhardt's solution, 1
749 mg/ml yeast tRNA, 100 μg/ml, salmon sperm DNA, 0.1% SDS) containing FISH probes at
750 50 °C for 10 h and then at 37 °C for an additional 10 h. After a series of wash steps, the
751 brains were dehydrated, cleared in xylene, and mounted in DPX. Image Z-stacks were
752 collected using an LSM880 confocal microscope fitted with an LD LCI Plan-Apochromat
753 25x/0.8 oil or Plan-Apochromat 63x/1.4 oil objective after the tissue cured for 24 h.
754

755 **RNA-Seq**

756 *Expression checks*

757 Neurons of interest were isolated by expressing a fluorescent protein, either mCD8-GFP
758 or tdTomato, using split-Gal4 drivers specific for particular cell types and then manually
759 picking the fluorescent neurons from dissociated brain tissue. As a preliminary to the
760 sorting process, each driver/reporter combination was 'expression checked' to determine
761 if the marked cells were sufficiently bright to sorted effectively and if there was any off-
762 target expression in neurons other than those of interest. Drivers that met both these
763 requirements were used in sorting experiments as described below.
764
765 *Sorting of fluorescent-labelled neurons*
766 *Drosophila* adults were collected daily as they eclosed, and aged 3-5 days prior to
767 dissection. For each sample, 60-100 brains were dissected in freshly prepared, ice cold
768 Adult Hemolymph Solution (AHS; 108 mM NaCl, 5 mM KCl, 2 mM $CaCl_2$, 8.2 mM
769 $MgCl_2$, 4 mM $NaHCO_3$, 1 mM NaH_2PO_4, 5 mM HEPES, 6 mM Trehalose, 10 mM
770 Sucrose), and the major tracheal branches removed. The brains were transferred to an 1.5
771 ml Eppendorf tube containing 500 microliters 1 mg/ml Liberase DH (Roche, prepared
772 according to the manufacturer's recommendation) in AHS, and digested for 1 h at room
773 temperature. The Liberase solution was removed and the brains washed three times with
774 ice cold AHS. The final wash was removed completely and 400 microliters of AHS+2%
775 Fetal Bovine Serum (FBS, Sigma) were added. The brain samples were gently triturated
776 with a series of fire-polished, FBS-coated Pasteur pipettes of descending pore sizes until
777 the tissue was homogenized, after which the tube was allowed to stand for 2-3 m so that
778 the larger debris could settle.

For hand sorting, the cell suspension was transferred to a Sylgard-lined Glass Bottom Dish (Willco Wells), leaving the debris at the bottom of the Eppendorf tube, and distributed evenly in a rectangular area in the center of the plate with the pipet tip. The cells were allowed to settle for 10-30 min prior to picking. Fluorescent cells were picked with a mouth aspirator consisting of a 0.8 mm Nalgene Syringe Filter (Thermo), a short stretch of tubing, a plastic needle holder, and a pulled Kwik-Fil Borosilicate Glass capillary (Fisher). Cells picked off the primary plate were transferred to a Sylgard-lined 35 mm Mat Tek Glass Bottom Microwell Dishes (Mat Tek) filled with 170 microliters AHS+2%FBS, allowed to settle, and then re-picked. Three washes were performed in this way before the purified cells were picked and transferred into 50 microliters buffer XB from the PicoPure RNA Isolation Kit (Life Technologies), lysed for 5 m at 42˚C, and stored at -80˚C.

For FACS sorting, the cell suspension was passed through a Falcon 5 ml round-bottom tube fitted with a 35 micrometer cell strainer cap (Fisher), and sorted on a Becton Dickson FACSAria II cell sorter, gated for single cells with a fluorescence intensity exceeding that of a non-fluorescent control. Positive events were sorted directly into 50 microliters PicoPure XB buffer, the sample lysed for 5 m at 42˚C, and stored at -80˚C.

Library preparation and sequencing

Total RNA was extracted from 100-500 pooled cells using the PicoPure kit (Life Technologies) according to the manufacturer's recommendation, including the on-column DNAse step. The extracted RNA was converted to cDNA and amplified with the Ovation RNA-Seq System V2 (NuGEN), and the yield quantified by NanoDrop

(Thermo). The cDNA was fragmented and the sequencing adaptors ligated onto the fragments using the Ovation Rapid Library System (NuGEN). Library quality and concentration was determined with the Kapa Illumina Library Quantification Kit (KK4854, Kapa Biosystems), and the libraries were pooled and sequenced on an Illumina NextSeq 550 with 75 base pair reads. Sequencing adapters were trimmed from the reads with Cutadapt (Martin, 2011) prior to alignment with STAR (Dobin et al., 2013) to the *Drosophila* r6.17 genome assembly on Flybase (Thurmond et al., 2019). The resulting transcript alignments were passed to RSEM (B. Li & Dewey, 2011) to generate gene expression counts.

Modeling

Inferring parameters of DA and NO plasticity

We assume that the immediate effects of DA-mediated and NO-mediated changes at a KC-to-MBON synapse are described by two variables d(t) and n(t), respectively. When the KC and corresponding DAN are coactive, these variables are modified according to:

$$\frac{d}{dt}d(t) = A_D\big(1 - d(t)\big)$$
$$\frac{d}{dt}n(t) = A_N\big(1 - n(t)\big) \quad (1)$$

When the DAN is active but the KC is inactive,

$$\frac{d}{dt}d(t) = -B_D d(t)$$
$$\frac{d}{dt}n(t) = -B_N n(t) \quad (2)$$

A and B determine how quickly the variables approach their maximum value of 1 or minimum value of 0.

To model the time it takes for the effects of synaptic plasticity to occur, we also define two additional variables

$$\tau_D \frac{d}{dt} D(t) = d(t) - D(t)$$
$$\tau_N \frac{d}{dt} N(t) = n(t) - N(t) \quad (3)$$

D(t) and N(t) follow the values of d(t) and n(t), but with slower timescales τD and τN respectively. Based on the data, we assume τD = 30 (s), and τN = 10 (min). This accounts for the slower induction of NO-mediated effects.

We start by inferring AD and AN from data by relating the values of D(t) and N(t) in our model to the activation of the MBON, and finally to the PI. We assume that the normalized KC-to-MBON synaptic weight is given by $w(t) \propto 1 - D(t)$ (DA-mediated depression) if NO is absent, or $w(t) \propto 1 + N(t)$ (NO-dependent facilitation) if DA is absent. In our model, odors A and B activate a random 10% of KCs (the results do not depend on the total number of KCs N_{KC}), and the activation of the MBON is given by r = $r = \frac{1}{N_{KC}} \sum_i w_i s_i$, where s_i = 1 if the ith KC is active and 0 otherwise. At the beginning of each trial, $D(t) = N(t) = 0$, so $w_i = 1$. If r_A and r_B are the MBON activations for odors A and B, then we assume the probability of the fly choosing odor A is equal to a softmax function of this activation:

$$P_{odorA} = \frac{e^{gr_A}}{e^{gr_A} + e^{gr_B}}$$

We also infer g, which determines how strongly the MBON activation influences the decision, with g = 0 corresponding to random choices.

We infer A_D, A_N, and g separately for DA-null and NO-null conditions. To do so, we determine the values of the parameters that minimize the mean squared distance between model prediction and experimentally measured PIs for the 1x 10s, 1x 1min, 3x 1min, and 10x 1min protocols (Figure 6B). This is accomplished by simulating the model defined by Equations Eq. 1 to Eq. 3 and calculating the resulting preference index using Equation Eq. 4. Optimal values for A_D, A_N, and g are found using a grid search. The optimization leads to $A_D = 4.3$ (min^{-1}) and $A_N = 0.96$ (min^{-1}) (the inferred values of g are similar for the two cases; 14.8 and 12.6, respectively). These values indicate that the DA effect saturates more quickly than the NO effect, nearly reaching its maximum effect after 1x 1min pairing.

Next, we model synaptic weights when both DA and NO-dependent changes occur. We consider two forms of interaction, an additive one with $w(t) \propto N(t) - D(t)$ and a multiplicative one with $w(t) \propto (1 - D(t))(1 + N(t))$. We use the values of A_D and A_N inferred previously but allow g to be readjusted to best match the data (for the multiplicative model, $g = 14.3$, similar to above, while for the additive model g = 24.6). Only the multiplicative model qualitatively matches the experimental data (Figure 8D).

Modeling memory decay after 1x 1 min pairing

Next, we ask how memory decays after a pairing protocol. We assume that, after the pairing protocol is complete, there is a background level of activity in the DANs, which leads to depression according to Eq. 2. We infer the values of B_D^{bg} and B_N^{bg} (where the superscript denotes decay due to background DAN activity) using a grid search to minimize the mean squared distance between the predicted and actual PI from Figure 6D. Other parameters are set to the

868 previously determined values using the multiplicative model above. This leads to B_D^{bg} =

869 2.7 (10^{-3} min^{-1}) and B_D^{bg} = 1.6 (10^{-3} min^{-1}).

870 *Predicting memory dynamics in reversal learning*

871 Finally, we also model the effects of different pairing protocols. We start by considering

872 DAN ac- tivation in the absence of odor. We infer values for B_D and B_N (different from

873 the background levels above, since DANs are now activated rather than at their

874 background levels of activation) by minimizing the mean squared difference between

875 predicted and actual PI for NO-null and DA-null conditions (Figure 7F), and with the

876 remaining parameters determined previously for the multi- plicative model. This yields

877 B_D = 0.26 (min^{-1}) and B_N = 0.16 (min^{-1}). These parameters are used to predict the

878 behavior during reversal learning (Figure 7F).

879

880

881

882

883

884

Supplemental Information

SUPPLEMENTAL FILE 1 RNA-seq data

SUPPLEMENTAL TABLE 1

Figure	Genotype	Drug and other treatments
Figure 1D top	*w, 20xUAS-CsChrimson-mVenus in attP18/w; R52H03-p65ADZp attP40/+; TH-ZpGAL4DBD in VK00027/+*	
Figure 1E top	*w, 20xUAS-CsChrimson-mVenus in attP18/w; R52H03-p65ADZp attP40/+; TH-ZpGAL4DBD in VK00027, ple2, DTHFS$^{+/-}$ in attP2/ ple2, DTHFS$^{+/-}$ in attP2*	
Figure 1F top	*w, 20xUAS-CsChrimson-mVenus in attP18/w; R52H03-p65ADZp attP40/+; TH-ZpGAL4DBD in VK00027, ple2, DTHFS$^{+/-}$ in attP2/ ple2, DTHFS$^{+/-}$ in attP2*	1mg/ml L-Dopa, 0.1 mg/ml S-(−)-Carbidopa for 12-16 hours
Figure 1G top	*w, 20xUAS-CsChrimson-mVenus in attP18/w; R52H03-p65ADZp attP40/UAS-dTH; TH-ZpGAL4DBD in VK00027, ple2, DTHFS$^{+/-}$ in attP2/ ple2, DTHFS$^{+/-}$ in attP2*	
Figure 1D bottom	*w, 20xUAS-CsChrimson-mVenus in attP18/w; R58E02-p65ADZp attP40/+; DDC-ZpGAL4DBD in VK00027/+*	
Figure 1E bottom	*w, 20xUAS-CsChrimson-mVenus in attP18/w; R58E02-p65ADZp attP40/+; DDC-ZpGAL4DBD in VK00027, ple2, DTHFS$^{+/-}$ in attP2/ ple2, DTHFS$^{+/-}$ in attP2*	
Figure 1F bottom	*w, 20xUAS-CsChrimson-mVenus in attP18/w; R58E02-p65ADZp attP40/+; DDC-ZpGAL4DBD in VK00027, ple2, DTHFS$^{+/-}$ in attP2/ ple2, DTHFS$^{+/-}$ in attP2*	1mg/ml L-Dopa, 0.1 mg/ml S-(−)-Carbidopa for 12-16 hours
Figure 1G bottom	*w, 20xUAS-CsChrimson-mVenus in attP18/w; R58E02-p65ADZp attP40/UAS-dTH; DDC-ZpGAL4DBD in VK00027, ple2, DTHFS$^{+/-}$ in attP2/ ple2, DTHFS$^{+/-}$ in attP2*	
Figure 1-figure supplement 1 PAM Wild type	*w, 20xUAS-CsChrimson-mVenus in attP18/w; R58E02-p65ADZp attP40/+; DDC-ZpGAL4DBD in VK00027/+*	
Figure 1- figure supplement 1 PAM Dopamine null	*w, 20xUAS-CsChrimson-mVenus in attP18/w; R58E02-p65ADZp attP40/+; DDC-ZpGAL4DBD in VK00027, ple2, DTHFS$^{+/-}$ in attP2/ ple2, DTHFS$^{+/-}$ in attP2*	
Figure 1- figure supplement 1 PAM Dopamine null TH rescue	*w, 20xUAS-CsChrimson-mVenus in attP18/w; R58E02-p65ADZp attP40/UAS-dTH; DDC-ZpGAL4DBD in VK00027, ple2, DTHFS$^{+/-}$ in attP2/ ple2, DTHFS$^{+/-}$ in attP2*	
Figure 1-figure supplement 1 PPL1 Dopamine null	*w, 20xUAS-CsChrimson-mVenus in attP18/w; R52H03-p65ADZp attP40/+; TH-ZpGAL4DBD in VK00027, ple2, DTHFS$^{+/-}$ in attP2/ ple2, DTHFS$^{+/-}$ in attP2*	
Figure 1- figure supplement 1 PPL1 TH rescue	*w, 20xUAS-CsChrimson-mVenus in attP18/w; R52H03-p65ADZp attP40/UAS-dTH; TH-ZpGAL4DBD in VK00027, ple2, DTHFS$^{+/-}$ in attP2/ ple2, DTHFS$^{+/-}$ in attP2*	
Figure 2	*w, 20xUAS-CsChrimson-mVenus in attP18/w; Gr66a-GAL4/+; +/ ple2, DTHFS$^{+/-}$ in attP2*	
Figure 2	*w, 20xUAS-CsChrimson-mVenus in attP18/w; Gr66a-GAL4/+; ple2, DTHFS$^{+/-}$ in attP2/ TH-ZpGAL4DBD in VK00027, ple2, DTHFS$^{+/-}$ in attP2*	
Figure 2	*w, 20xUAS-CsChrimson-mVenus in attP18/w; R52H03-p65ADZp attP40/+; +/TH-ZpGAL4DBD in VK00027, ple2, DTHFS$^{+/-}$ in attP2*	
Figure 2	*w, 20xUAS-CsChrimson-mVenus in attP18/w; R52H03-p65ADZp attP40/+; ple2, DTHFS$^{+/-}$ in attP2/TH-ZpGAL4DBD in VK00027, ple2, DTHFS$^{+/-}$ in attP2*	
Figure 2	*w, 13xLeXAop-CsChrimson-tdTomato attp18/w; VT045661-LexA JK22C/+; +/TH-ZpGAL4DBD in VK00027, ple2, DTHFS$^{+/-}$ in attP2*	
Figure 2	*w, 13xLeXAop-CsChrimson-tdTomato attp18/w; VT045661-LexA JK22C/+; ple2, DTHFS$^{+/-}$ in attP2/ TH-ZpGAL4DBD in VK00027, ple2, DTHFS$^{+/-}$ in attP2*	
Figure 2	*w, 20xUAS-CsChrimson-mVenus in attP18/w; R73F07-p65ADZp attP40/+; +/TH-ZpGAL4DBD in VK00027, ple2, DTHFS$^{+/-}$ in attP2*	
Figure 2	*w, 20xUAS-CsChrimson-mVenus in attP18/w; R73F07-p65ADZp attP40/+; ple2, DTHFS$^{+/-}$ in attP2/TH-ZpGAL4DBD in VK00027, ple2, DTHFS$^{+/-}$ in attP2*	
Figure 2	*w, 20xUAS-CsChrimson-mVenus in attP18/w; R72B05-p65ADZp attP40/+; +/TH-ZpGAL4DBD in VK00027, ple2, DTHFS$^{+/-}$ in attP2*	

Figure 2	*w, 20xUAS-CsChrimson-mVenus in attP18/w; R72B05-p65ADZp attP40/+; ple2, DTHFS$^{+/-}$ in attP2/TH-ZpGAL4DBD in VK00027, ple2, DTHFS$^{+/-}$ in attP2*	
Figure 2	*w, 20xUAS-CsChrimson-mVenus in attP18/w; R24E12-p65ADZp attP40/+; +/DDC-ZpGAL4DBD in VK00027, ple2, DTHFS$^{+/-}$ in attP2*	
Figure 2	*w, 20xUAS-CsChrimson-mVenus in attP18/w; R24E12-p65ADZp attP40/+; ple2, DTHFS$^{+/-}$ in attP2/DDC-ZpGAL4DBD in VK00027, ple2, DTHFS$^{+/-}$ in attP2*	
Figure 2	*w, 20xUAS-CsChrimson-mVenus in attP18/w; R58E02-p65ADZp attP40/+; TH-ZpGAL4DBD in VK00027/+*	
Figure 2	*w, 20xUAS-CsChrimson-mVenus in attP18/w; R58E02-p65ADZp attP40/+; ple2, DTHFS$^{+/-}$ in attP2/TH-ZpGAL4DBD in VK00027, ple2, DTHFS$^{+/-}$ in attP2*	
Figure 2	*w, 20xUAS-CsChrimson-mVenus in attP18/w; R58E02-p65ADZp attP40/+; +/DDC-ZpGAL4DBD in VK00027, ple2, DTHFS$^{+/-}$ in attP2*	
Figure 2	*w, 20xUAS-CsChrimson-mVenus in attP18/w; R58E02-p65ADZp attP40/+; ple2, DTHFS$^{+/-}$ in attP2/DDC-ZpGAL4DBD in VK00027, ple2, DTHFS$^{+/-}$ in attP2*	
Figure 2- figure supplement 1 left	*w, 20xUAS-CsChrimson-mVenus in attP18/w; R73F07-p65ADZp attP40/+; +/TH-ZpGAL4DBD in VK00027, ple2, DTHFS$^{+/-}$ in attP2*	
Figure 2- figure supplement 1 center	*w, 20xUAS-CsChrimson-mVenus in attP18/w; R72B05-p65ADZp attP40/+; +/TH-ZpGAL4DBD in VK00027, ple2, DTHFS$^{+/-}$ in attP2*	
Figure 2- figure supplement 1 right	*w, 20xUAS-CsChrimson-mVenus in attP18/w; R24E12-p65ADZp attP40/+; +/DDC-ZpGAL4DBD in VK00027, ple2, DTHFS$^{+/-}$ in attP2*	
Figure 3D	*w, 20xUAS-CsChrimson-mVenus in attP18/w;;+/MB320C*	
Figure 3E	*CS*	
Figure 3-figure supplement 1B	*w, 20xUAS-CsChrimson-mVenus in attP18/w;; background attP2 (BDSC#36303)/MB320C*	
Figure 3-figure supplement 1B	*w, 20xUAS-CsChrimson-mVenus in attP18/w;; UAS-NOS-shRNA HMC03076 in attP2/MB320C*	
Figure 3-figure supplement 1C	*CS*	
Figure 3- figure supplement 1D	*w/w; UAS-7xHalo7::CAAX in attP40/+;MB320C/+*	
Figure 4A	*w, 13xLeXAop-CsChrimson-tdTomato attp18/w; VT045661-LexA JK22C/+; ple2, DTHFS$^{+/-}$ in attP2/TH-ZpGAL4DBD in VK00027, ple2, DTHFS$^{+/-}$ in attP2*	0-100 mM L-NNA, 100 mM L-NNA + 1mg/ml L-Dopa, 0.1 mg/ml S-(−)-Carbidopa, or 1mg/ml L-Dopa, 0.1 mg/ml S-(−)-Carbidopa for 12-16 hours
Figure 4B left	*w, 20xUAS-CsChrimson-mVenus in attP18/w; R58E02-p65ADZp attP40/+; TH-ZpGAL4DBD in VK00027, ple2, DTHFS$^{+/-}$ in attP2/ ple2, DTHFS$^{+/-}$ in attP2*	0 or 100 mM L-NNA for 12-16 hours
Figure 4B right	*w, 20xUAS-CsChrimson-mVenus in attP18/w; R73F07-p65ADZp attP40/+; TH-ZpGAL4DBD in VK00027, ple2, DTHFS$^{+/-}$ in attP2/ ple2, DTHFS$^{+/-}$ in attP2*	0 or 100 mM L-NNA for 12-16 hours
Figure 4C left	*w, 20xUAS-CsChrimson-mVenus in attP18/w; R52H03-p65ADZp attP40/background control attP40; TH-ZpGAL4DBD in VK00027, ple2, DTHFS$^{+/-}$ in attP2/ ple2, DTHFS$^{+/-}$ in attP2*	
Figure 4C right	*w, 20xUAS-CsChrimson-mVenus in attP18/w; R52H03-p65ADZp attP40/UAS-NOS-shRNA in attP40; TH-ZpGAL4DBD in VK00027, ple2, DTHFS$^{+/-}$ in attP2/ ple2, DTHFS$^{+/-}$ in attP2*	
Figure 4D and E left	*w, 20xUAS-CsChrimson-mVenus in attP18/w; R72B05-p65ADZp attP40/+; TH-ZpGAL4DBD in VK00027, ple2, DTHFS$^{+/-}$ in attP2/ ple2, DTHFS$^{+/-}$ in attP2*	
Figure 4D and E right	*w, 20xUAS-CsChrimson-mVenus in attP18/w; R72B05-p65ADZp attP40/UAS-NOS; TH-ZpGAL4DBD in VK00027, ple2, DTHFS$^{+/-}$ in attP2/ ple2, DTHFS$^{+/-}$ in attP2*	
Figure 5C left	*w, 13xLeXAop-CsChrimson-tdTomato attp18/w; VT045661-LexA JK22C/background control attp40;MB-switch-GAL4, ple2, DTHFS$^{+/-}$ in attP2 /ple2, DTHFS$^{+/-}$ in attP2*	0 or 1.5 mg/mL RU486 for 2 days
Figure 5C center	*w, 13xLeXAop-CsChrimson-tdTomato attp18/w; VT045661-LexA JK22C/UAS-Gycbeta100B-shRNA in attp40;MB-switch-GAL4, ple2, DTHFS$^{+/-}$ in attP2 /ple2, DTHFS$^{+/-}$ in attP2*	0 or 1.5 mg/mL RU486 for 2 days
Figure 5C right	*w, 13xLeXAop-CsChrimson-tdTomato attp18/w; VT045661-LexA JK22C/UAS-Gycbeta100B-shRNA in attp40;MB-switch-GAL4, ple2, DTHFS$^{+/-}$ in attP2 /ple2, DTHFS$^{+/-}$ in attP2*	0 or 1.5 mg/mL RU486 and 1mg/ml L-Dopa, 0.1 mg/ml S-(−)-Carbidopa for 2 days
Figure 5- figure supplement 1 left	*yw;Gycbeta100B[MI08892-GFSTF.2]*	
Figure 5- figure supplement 1 right	*CS*	

Figure 6B Wild Type	*w, 13xLeXAop-CsChrimson-tdTomato attp18/w; VT045661-LexA JK22C/+; /+; +/+*	
Figure 6B L-NNA	*w, 13xLeXAop-CsChrimson-tdTomato attp18/w; VT045661-LexA JK22C/+; /+; +/+*	100mM L-NNA for 12-16 hours
Figure 6B DA null	*w, 13xLeXAop-CsChrimson-tdTomato attp18/w; VT045661-LexA JK22C/+; ple2, DTHFS$^{+/-}$ in attP2/TH-ZpGAL4DBD in VK00027, ple2, DTHFS$^{+/-}$ in attP2*	
Figure 6C	*w, 13xLeXAop-CsChrimson-tdTomato attp18/w; VT045661-LexA JK22C/+; ple2, DTHFS$^{+/-}$ in attP2/TH-ZpGAL4DBD in VK00027, ple2, DTHFS$^{+/-}$ in attP2*	
Figure 6D	*w, 20xUAS-CsChrimson-mVenus in attP18/w;; background attP2 (BDSC#36303)/MB320C*	
Figure 6D	*w, 20xUAS-CsChrimson-mVenus in attP18/w;; UAS-NOS-shRNA HMC03076 in attP2/MB320C*	
Figure 6E left	*w, 20xUAS-CsChrimson-mVenus in attP18/yw;; background attP2 (BDSC#36303)/MB320C*	
Figure 6E center	*w, 20xUAS-CsChrimson-mVenus in attP18/yw;; UAS-NOS-shRNA HMC03076 in attP2/MB320C*	
Figure 6E right	*w, 13xLeXAop-CsChrimson-tdTomato attp18/w; VT045661-LexA JK22C/+; ple2, DTHFS$^{+/-}$ in attP2/TH-ZpGAL4DBD in VK00027, ple2, DTHFS$^{+/-}$ in attP2*	
Figure 6-figure supplement 1A	*w, 13xLeXAop-CsChrimson-tdTomato attp18/w; VT045661-LexA JK22C/+; +/+*	
Figure 6-figure supplement 1B control	*w/yw;; background attP2 (BDSC#36303)/MB320C*	
Figure 6- figure supplement 1B NOS-RNAi	*w/yw;;UAS-NOS-shRNA HMC03076 in attP2/MB320C*	
Figure 6- figure supplement 1C	*w, 13xLeXAop-CsChrimson-tdTomato attp18/w; VT045661-LexA JK22C/+; +/+*	0 or 100mM L-NNA for 12-16 hours
Figure 7B-E Wild Type	*w, 13xLeXAop-CsChrimson-tdTomato attp18/w; VT045661-LexA JK22C/+; /+; +/+*	
Figure 7B-E L-NNA	*w, 13xLeXAop-CsChrimson-tdTomato attp18/w; VT045661-LexA JK22C/+; /+; +/+*	100mM L-NNA for 12-16 hours
Figure 7B-E DA null	*w, 13xLeXAop-CsChrimson-tdTomato attp18/w; VT045661-LexA JK22C/+; ple2, DTHFS$^{+/-}$ in attP2/TH-ZpGAL4DBD in VK00027, ple2, DTHFS$^{+/-}$ in attP2*	

890

891

892

893

894 **References**

895

896 Abrams, T. W., Yovell, Y., Onyike, C. U., Cohen, J. E., & Jarrard, H. E. (1998). Analysis of
897 sequence-dependent interactions between transient calcium and transmitter
898 stimuli in activating adenylyl cyclase in Aplysia: possible contribution to CS--
899 US sequence requirement during conditioning. *Learn Mem, 4*(6), 496-509.
900 Abu-Soud, H. M., & Stuehr, D. J. (1993). Nitric oxide synthases reveal a role for
901 calmodulin in controlling electron transfer. *Proc Natl Acad Sci U S A, 90*(22),
902 10769-10772.
903 Akalal, D. B., Wilson, C. F., Zong, L., Tanaka, N. K., Ito, K., & Davis, R. L. (2006). Roles
904 for Drosophila mushroom body neurons in olfactory learning and memory.
905 *Learn Mem, 13*(5), 659-668. doi:10.1101/lm.221206
906 Aso, Y., Hattori, D., Yu, Y., Johnston, R. M., Iyer, N. A., Ngo, T. T., . . . Rubin, G. M.
907 (2014). The neuronal architecture of the mushroom body provides a logic for
908 associative learning. *Elife, 3*, e04577. doi:10.7554/eLife.04577
909 Aso, Y., Herb, A., Ogueta, M., Siwanowicz, I., Templier, T., Friedrich, A. B., . . .
910 Tanimoto, H. (2012). Three dopamine pathways induce aversive odor
911 memories with different stability. *PLoS Genet, 8*(7), e1002768.
912 doi:10.1371/journal.pgen.1002768
913 Aso, Y., & Rubin, G. M. (2016). Dopaminergic neurons write and update memories
914 with cell-type-specific rules. *Elife, 5*. doi:10.7554/eLife.16135
915 Aso, Y., Sitaraman, D., Ichinose, T., Kaun, K. R., Vogt, K., Belliart-Guerin, G., . . . Rubin,
916 G. M. (2014). Mushroom body output neurons encode valence and guide
917 memory-based action selection in Drosophila. *Elife, 3*, e04580.
918 doi:10.7554/eLife.04580
919 Aso, Y., Siwanowicz, I., Bracker, L., Ito, K., Kitamoto, T., & Tanimoto, H. (2010).
920 Specific dopaminergic neurons for the formation of labile aversive memory.
921 *Curr Biol, 20*(16), 1445-1451. doi:10.1016/j.cub.2010.06.048
922 Berry, J. A., Cervantes-Sandoval, I., Nicholas, E. P., & Davis, R. L. (2012). Dopamine is
923 required for learning and forgetting in Drosophila. *Neuron, 74*(3), 530-542.
924 doi:10.1016/j.neuron.2012.04.007
925 Berry, J. A., Phan, A., & Davis, R. L. (2018). Dopamine Neurons Mediate Learning and
926 Forgetting through Bidirectional Modulation of a Memory Trace. *Cell Rep,*
927 *25*(3), 651-662 e655. doi:10.1016/j.celrep.2018.09.051
928 Blum, A. L., Li, W., Cressy, M., & Dubnau, J. (2009). Short- and long-term memory in
929 Drosophila require cAMP signaling in distinct neuron types. *Curr Biol, 19*(16),
930 1341-1350. doi:10.1016/j.cub.2009.07.016
931 Blum, A. L., Li, W. H., Cressy, M., & Dubnau, J. (2009). Short- and Long-Term Memory
932 in Drosophila Require cAMP Signaling in Distinct Neuron Types. *Current*
933 *Biology, 19*(16), 1341-1350. doi:Doi 10.1016/J.Cub.2009.07.016
934 Boto, T., Louis, T., Jindachomthong, K., Jalink, K., & Tomchik, S. M. (2014).
935 Dopaminergic modulation of cAMP drives nonlinear plasticity across the

936 Drosophila mushroom body lobes. *Curr Biol, 24*(8), 822-831.
937 doi:10.1016/j.cub.2014.03.021
938 Bouzaiane, E., Trannoy, S., Scheunemann, L., Placais, P. Y., & Preat, T. (2015). Two
939 independent mushroom body output circuits retrieve the six discrete
940 components of Drosophila aversive memory. *Cell Rep, 11*(8), 1280-1292.
941 doi:10.1016/j.celrep.2015.04.044
942 Bredt, D. S., Hwang, P. M., & Snyder, S. H. (1990). Localization of nitric oxide
943 synthase indicating a neural role for nitric oxide. *Nature, 347*(6295), 768-
944 770. doi:10.1038/347768a0
945 Burke, C. J., Huetteroth, W., Owald, D., Perisse, E., Krashes, M. J., Das, G., . . . Waddell,
946 S. (2012). Layered reward signalling through octopamine and dopamine in
947 Drosophila. *Nature, 492*(7429), 433-437. doi:10.1038/nature11614
948 Byrne, J. H., Baxter, D. A., Buonomano, D. V., Cleary, L. J., Eskin, A., Goldsmith, J. R., . . .
949 Scholz, K. P. (1991). Neural and molecular bases of nonassociative and
950 associative learning in Aplysia. *Ann N Y Acad Sci, 627*, 124-149.
951 Cassenaer, S., & Laurent, G. (2012). Conditional modulation of spike-timing-
952 dependent plasticity for olfactory learning. *Nature, 482*(7383), 47-U62.
953 doi:Doi 10.1038/Nature10776
954 Cervantes-Sandoval, I., Chakraborty, M., MacMullen, C., & Davis, R. L. (2016).
955 Scribble Scaffolds a Signalosome for Active Forgetting. *Neuron, 90*(6), 1230-
956 1242. doi:10.1016/j.neuron.2016.05.010
957 Chen, Y., Saulnier, J. L., Yellen, G., & Sabatini, B. L. (2014). A PKA activity sensor for
958 quantitative analysis of endogenous GPCR signaling via 2-photon FRET-FLIM
959 imaging. *Front Pharmacol, 5*, 56. doi:10.3389/fphar.2014.00056
960 Cichewicz, K., Garren, E. J., Adiele, C., Aso, Y., Wang, Z., Wu, M., . . . Hirsh, J. (2016). A
961 new brain dopamine-deficient Drosophila and its pharmacological and
962 genetic rescue. *Genes Brain Behav*. doi:10.1111/gbb.12353
963 Claridge-Chang, A., Roorda, R. D., Vrontou, E., Sjulson, L., Li, H., Hirsh, J., &
964 Miesenbock, G. (2009). Writing memories with light-addressable
965 reinforcement circuitry. *Cell, 139*(2), 405-415. doi:10.1016/j.cell.2009.08.034
966 Cohn, R., Morantte, I., & Ruta, V. (2015). Coordinated and Compartmentalized
967 Neuromodulation Shapes Sensory Processing in Drosophila. *Cell, 163*(7),
968 1742-1755. doi:10.1016/j.cell.2015.11.019
969 Croset, V., Treiber, C. D., & Waddell, S. (2018). Cellular diversity in the Drosophila
970 midbrain revealed by single-cell transcriptomics. *Elife, 7*.
971 doi:10.7554/eLife.34550
972 Das, G., Klappenbach, M., Vrontou, E., Perisse, E., Clark, C. M., Burke, C. J., & Waddell,
973 S. (2014). Drosophila learn opposing components of a compound food
974 stimulus. *Curr Biol, 24*(15), 1723-1730. doi:10.1016/j.cub.2014.05.078
975 Davis, R. L., Cherry, J., Dauwalder, B., Han, P. L., & Skoulakis, E. (1995). The cyclic
976 AMP system and Drosophila learning. *Mol Cell Biochem, 149-150*, 271-278.
977 Debelle, J. S., & Heisenberg, M. (1994). Associative Odor Learning in Drosophila
978 Abolished by Chemical Ablation of Mushroom Bodies. *Science, 263*(5147),
979 692-695. doi:Doi 10.1126/Science.8303280

Dobin, A., Davis, C. A., Schlesinger, F., Drenkow, J., Zaleski, C., Jha, S., . . . Gingeras, T. R. (2013). STAR: ultrafast universal RNA-seq aligner. *Bioinformatics, 29*(1), 15-21. doi:10.1093/bioinformatics/bts635

Dubnau, J., Grady, L., Kitamoto, T., & Tully, T. (2001). Disruption of neurotransmission in Drosophila mushroom body blocks retrieval but not acquisition of memory. *Nature, 411*(6836), 476-480. doi:10.1038/35078077

Eichler, K., Li, F., Litwin-Kumar, A., Park, Y., Andrade, I., Schneider-Mizell, C. M., . . . Cardona, A. (2017). The complete connectome of a learning and memory centre in an insect brain. *Nature, 548*(7666), 175-182. doi:10.1038/nature23455

Erber, J., MASUHR, T., & MENZEL, R. (1980). Localization of short-term memory in the brain of the bee, Apis mellifera. *Physiological Entomology, 5*(4). doi:10.1111/j.1365-3032.1980.tb00244.x

Eroglu, E., Gottschalk, B., Charoensin, S., Blass, S., Bischof, H., Rost, R., . . . Malli, R. (2016). Development of novel FP-based probes for live-cell imaging of nitric oxide dynamics. *Nat Commun, 7*, 10623. doi:10.1038/ncomms10623

Farris, S. M. (2011). Are mushroom bodies cerebellum-like structures? *Arthropod Struct Dev, 40*(4), 368-379. doi:10.1016/j.asd.2011.02.004

Fred P. Davis1, *,X, Aljoscha Nern1,*, Serge Picard1,3, Michael B. Reiser1, Gerald M. Rubin1, Sean R. Eddy1,4, and Gilbert L. Henry1,5,X. (2018). A genetic, genomic, and computational resource for exploring neural circuit function. *bioRxiv*.

Galili, D. S., Dylla, K. V., Ludke, A., Friedrich, A. B., Yamagata, N., Wong, J. Y., . . . Tanimoto, H. (2014). Converging circuits mediate temperature and shock aversive olfactory conditioning in Drosophila. *Curr Biol, 24*(15), 1712-1722. doi:10.1016/j.cub.2014.06.062

Gervasi, N., Tchenio, P., & Preat, T. (2010). PKA dynamics in a Drosophila learning center: coincidence detection by rutabaga adenylyl cyclase and spatial regulation by dunce phosphodiesterase. *Neuron, 65*(4), 516-529. doi:10.1016/j.neuron.2010.01.014

Han, K. A., Millar, N. S., Grotewiel, M. S., & Davis, R. L. (1996). DAMB, a novel dopamine receptor expressed specifically in Drosophila mushroom bodies. *Neuron, 16*(6), 1127-1135.

Heisenberg, M. (2003). Mushroom body memoir: From maps to models. *Nature Reviews Neuroscience, 4*(4), 266-275. doi:Doi 10.1038/Nrn1074

Herry, C., & Johansen, J. P. (2014). Encoding of fear learning and memory in distributed neuronal circuits. *Nat Neurosci, 17*(12), 1644-1654. doi:10.1038/nn.3869

Hige, T., Aso, Y., Modi, M. N., Rubin, G. M., & Turner, G. C. (2015). Heterosynaptic Plasticity Underlies Aversive Olfactory Learning in Drosophila. *Neuron, 88*(5), 985-998. doi:10.1016/j.neuron.2015.11.003

Huetteroth, W., Perisse, E., Lin, S., Klappenbach, M., Burke, C., & Waddell, S. (2015). Sweet taste and nutrient value subdivide rewarding dopaminergic neurons in Drosophila. *Curr Biol, 25*(6), 751-758. doi:10.1016/j.cub.2015.01.036

Ichinose, T., Aso, Y., Yamagata, N., Abe, A., Rubin, G. M., & Tanimoto, H. (2015). Reward signal in a recurrent circuit drives appetitive long-term memory formation. *Elife, 4*. doi:10.7554/eLife.10719

Isabel, G., Pascual, A., & Preat, T. (2004). Exclusive consolidated memory phases in Drosophila. *Science, 304*(5673), 1024-1027. doi:10.1126/science.1094932

Kanao, T., Sawada, T., Davies, S. A., Ichinose, H., Hasegawa, K., Takahashi, R., . . . Imai, Y. (2012). The nitric oxide-cyclic GMP pathway regulates FoxO and alters dopaminergic neuron survival in Drosophila. *PLoS One, 7*(2), e30958. doi:10.1371/journal.pone.0030958

Keene, A. C., & Waddell, S. (2007). Drosophila olfactory memory: single genes to complex neural circuits. *Nature Reviews Neuroscience, 8*(5), 341-354. doi:Doi 10.1038/Nrn2098

Kim, Y. C., Lee, H. G., & Han, K. A. (2007). D1 dopamine receptor dDA1 is required in the mushroom body neurons for aversive and appetitive learning in Drosophila. *J Neurosci, 27*(29), 7640-7647. doi:10.1523/JNEUROSCI.1167-07.2007

Kirkhart, C., & Scott, K. (2015). Gustatory learning and processing in the Drosophila mushroom bodies. *J Neurosci, 35*(15), 5950-5958. doi:10.1523/JNEUROSCI.3930-14.2015

Knapek, S., Sigrist, S., & Tanimoto, H. (2011). Bruchpilot, a synaptic active zone protein for anesthesia-resistant memory. *J Neurosci, 31*(9), 3453-3458. doi:10.1523/JNEUROSCI.2585-10.2011

Kosakai, K., Tsujiuchi, Y., & Yoshino, M. (2015). Nitric oxide augments single Ca(2+) channel currents via cGMP-dependent protein kinase in Kenyon cells isolated from the mushroom body of the cricket brain. *J Insect Physiol, 78*, 26-32. doi:10.1016/j.jinsphys.2015.04.009

Krashes, M. J., DasGupta, S., Vreede, A., White, B., Armstrong, J. D., & Waddell, S. (2009). A Neural Circuit Mechanism Integrating Motivational State with Memory Expression in Drosophila. *Cell, 139*(2), 416-427. doi:Doi 10.1016/J.Cell.2009.08.035

Kruttner, S., Traunmuller, L., Dag, U., Jandrasits, K., Stepien, B., Iyer, N., . . . Keleman, K. (2015). Synaptic Orb2A Bridges Memory Acquisition and Late Memory Consolidation in Drosophila. *Cell Rep, 11*(12), 1953-1965. doi:10.1016/j.celrep.2015.05.037

Kuntz, S., Poeck, B., & Strauss, R. (2017). Visual Working Memory Requires Permissive and Instructive NO/cGMP Signaling at Presynapses in the Drosophila Central Brain. *Curr Biol, 27*(5), 613-623. doi:10.1016/j.cub.2016.12.056

Lev-Ram, V., Wong, S. T., Storm, D. R., & Tsien, R. Y. (2002). A new form of cerebellar long-term potentiation is postsynaptic and depends on nitric oxide but not cAMP. *Proc Natl Acad Sci U S A, 99*(12), 8389-8393. doi:10.1073/pnas.122206399

Li, B., & Dewey, C. N. (2011). RSEM: accurate transcript quantification from RNA-Seq data with or without a reference genome. *BMC Bioinformatics, 12*, 323. doi:10.1186/1471-2105-12-323

Li, Y., & van den Pol, A. N. (2006). Differential target-dependent actions of coexpressed inhibitory dynorphin and excitatory hypocretin/orexin neuropeptides. *J Neurosci, 26*(50), 13037-13047. doi:10.1523/JNEUROSCI.3380-06.2006

Lin, S., Owald, D., Chandra, V., Talbot, C., Huetteroth, W., & Waddell, S. (2014). Neural correlates of water reward in thirsty Drosophila. *Nat Neurosci, 17*(11), 1536-1542. doi:10.1038/nn.3827

Liu, C., Placais, P. Y., Yamagata, N., Pfeiffer, B. D., Aso, Y., Friedrich, A. B., . . . Tanimoto, H. (2012). A subset of dopamine neurons signals reward for odour memory in Drosophila. *Nature, 488*(7412), 512-516. doi:10.1038/nature11304

Long, X., Colonell, J., Wong, A. M., Singer, R. H., & Lionnet, T. (2017). Quantitative mRNA imaging throughout the entire Drosophila brain. *Nature Methods, 14*(7), 703-706. doi:10.1038/nmeth.4309

Love, M. I., Huber, W., & Anders, S. (2014). Moderated estimation of fold change and dispersion for RNA-seq data with DESeq2. *Genome Biol, 15*(12), 550. doi:10.1186/s13059-014-0550-8

Maher, B. J., & Westbrook, G. L. (2008). Co-transmission of dopamine and GABA in periglomerular cells. *J Neurophysiol, 99*(3), 1559-1564. doi:10.1152/jn.00636.2007

Mao, Z., & Davis, R. L. (2009). Eight different types of dopaminergic neurons innervate the Drosophila mushroom body neuropil: anatomical and physiological heterogeneity. *Front Neural Circuits, 3*, 5. doi:10.3389/neuro.04.005.2009

Mao, Z., Roman, G., Zong, L., & Davis, R. L. (2004). Pharmacogenetic rescue in time and space of the rutabaga memory impairment by using Gene-Switch. *Proc Natl Acad Sci U S A, 101*(1), 198-203. doi:10.1073/pnas.0306128101

Marr, D. (1969). A theory of cerebellar cortex. *J Physiol, 202*(2), 437-470.

Martin, M. (2011). Cutadapt Removes Adapter Sequences From High-Throughput Sequencing Reads. *EMBnet.journal, Vol.17, No,1*. doi:https://doi.org/10.14806/ej.17.1.200

McGuire, S. E., Deshazer, M., & Davis, R. L. (2005). Thirty years of olfactory learning and memory research in Drosophila melanogaster. *Prog Neurobiol, 76*(5), 328-347. doi:Doi 10.1016/J.Pneurobio.2005.09.003

McGuire, S. E., Le, P. T., & Davis, R. L. (2001). The role of Drosophila mushroom body signaling in olfactory memory. *Science, 293*(5533), 1330-1333. doi:10.1126/science.1062622

McGuire, S. E., Le, P. T., Osborn, A. J., Matsumoto, K., & Davis, R. L. (2003). Spatiotemporal rescue of memory dysfunction in Drosophila. *Science, 302*(5651), 1765-1768. doi:10.1126/science.1089035

Medina, J. F., Repa, J. C., Mauk, M. D., & LeDoux, J. E. (2002). Parallels between cerebellum and amygdala-dependent conditioning. *Nature Reviews Neuroscience, 3*(2), 122-131. doi:Doi 10.1038/Nrn728

Meissner, G. W., Nern, A., Singer, R. H., Wong, A. M., Malkesman, O., & Long, X. (2019). Mapping Neurotransmitter Identity in the Whole-Mount Drosophila Brain Using Multiplex High-Throughput Fluorescence in Situ Hybridization. *Genetics, 211*(2), 473-482. doi:10.1534/genetics.118.301749

Morton, D. B., Langlais, K. K., Stewart, J. A., & Vermehren, A. (2005). Comparison of the properties of the five soluble guanylyl cyclase subunits in Drosophila melanogaster. *J Insect Sci, 5*, 12.

Ni, J. Q., Zhou, R., Czech, B., Liu, L. P., Holderbaum, L., Yang-Zhou, D., . . . Perrimon, N. (2011). A genome-scale shRNA resource for transgenic RNAi in Drosophila. *Nature Methods, 8*(5), 405-407. doi:10.1038/nmeth.1592

Niens, J., Reh, F., Coban, B., Cichewicz, K., Eckardt, J., Liu, Y. T., . . . Riemensperger, T. D. (2017). Dopamine Modulates Serotonin Innervation in the Drosophila Brain. *Front Syst Neurosci, 11*, 76. doi:10.3389/fnsys.2017.00076

Niewalda, T., Michels, B., Jungnickel, R., Diegelmann, S., Kleber, J., Kahne, T., & Gerber, B. (2015). Synapsin Determines Memory Strength after Punishment- and Relief-Learning. *Journal of Neuroscience, 35*(19), 7487-7502. doi:10.1523/Jneurosci.4454-14.2015

Nusbaum, M. P., Blitz, D. M., & Marder, E. (2017). Functional consequences of neuropeptide and small-molecule co-transmission. *Nat Rev Neurosci, 18*(7), 389-403. doi:10.1038/nrn.2017.56

Okada, R., Rybak, J., Manz, G., & Menzel, R. (2007). Learning-related plasticity in PE1 and other mushroom body-extrinsic neurons in the honeybee brain. *J Neurosci, 27*(43), 11736-11747. doi:10.1523/JNEUROSCI.2216-07.2007

Owald, D., Felsenberg, J., Talbot, C. B., Das, G., Perisse, E., Huetteroth, W., & Waddell, S. (2015). Activity of defined mushroom body output neurons underlies learned olfactory behavior in Drosophila. *Neuron, 86*(2), 417-427. doi:10.1016/j.neuron.2015.03.025

Pai, T. P., Chen, C. C., Lin, H. H., Chin, A. L., Lai, J. S., Lee, P. T., . . . Chiang, A. S. (2013). Drosophila ORB protein in two mushroom body output neurons is necessary for long-term memory formation. *Proc Natl Acad Sci U S A, 110*(19), 7898-7903. doi:10.1073/pnas.1216336110

Patriarchi, T., Cho, J. R., Merten, K., Howe, M. W., Marley, A., Xiong, W. H., . . . Tian, L. (2018). Ultrafast neuronal imaging of dopamine dynamics with designed genetically encoded sensors. *Science, 360*(6396). doi:10.1126/science.aat4422

Pavot, P., Carbognin, E., & Martin, J. R. (2015). PKA and cAMP/CNG Channels Independently Regulate the Cholinergic Ca(2+)-Response of Drosophila Mushroom Body Neurons(1,2,3). *eNeuro, 2*(2). doi:10.1523/ENEURO.0054-14.2015

Pettersson, J. (1970). *Insect Systematics & Evolution, 1* (1), 63 – 73. doi:10.1163/187631270X00357

Placais, P. Y., Trannoy, S., Friedrich, A. B., Tanimoto, H., & Preat, T. (2013). Two pairs of mushroom body efferent neurons are required for appetitive long-term memory retrieval in Drosophila. *Cell Rep, 5*(3), 769-780. doi:10.1016/j.celrep.2013.09.032

Poulin, J. F., Zou, J., Drouin-Ouellet, J., Kim, K. Y., Cicchetti, F., & Awatramani, R. B. (2014). Defining midbrain dopaminergic neuron diversity by single-cell gene expression profiling. *Cell Rep, 9*(3), 930-943. doi:10.1016/j.celrep.2014.10.008

Qin, H., Cressy, M., Li, W., Coravos, J. S., Izzi, S. A., & Dubnau, J. (2012). Gamma neurons mediate dopaminergic input during aversive olfactory memory formation in Drosophila. *Curr Biol, 22*(7), 608-614. doi:10.1016/j.cub.2012.02.014

Quinn, W. G., Harris, W. A., & Benzer, S. (1974). Conditioned behavior in Drosophila melanogaster. *Proc Natl Acad Sci U S A, 71*(3), 708-712.

Rabinovich, D., Yaniv, S. P., Alyagor, I., & Schuldiner, O. (2016). Nitric Oxide as a Switching Mechanism between Axon Degeneration and Regrowth during Developmental Remodeling. *Cell, 164*(1-2), 170-182. doi:10.1016/j.cell.2015.11.047

Regulski, M., & Tully, T. (1995). Molecular and biochemical characterization of dNOS: a Drosophila Ca2+/calmodulin-dependent nitric oxide synthase. *Proc Natl Acad Sci U S A, 92*(20), 9072-9076.

Riemensperger, T., Isabel, G., Coulom, H., Neuser, K., Seugnet, L., Kume, K., . . . Birman, S. (2011). Behavioral consequences of dopamine deficiency in the Drosophila central nervous system. *Proc Natl Acad Sci U S A, 108*(2), 834-839. doi:10.1073/pnas.1010930108

Riemensperger, T., Voller, T., Stock, P., Buchner, E., & Fiala, A. (2005). Punishment prediction by dopaminergic neurons in Drosophila. *Curr Biol, 15*(21), 1953-1960. doi:10.1016/j.cub.2005.09.042

Schindelin, J., Arganda-Carreras, I., Frise, E., Kaynig, V., Longair, M., Pietzsch, T., . . . Cardona, A. (2012). Fiji: an open-source platform for biological-image analysis. *Nature Methods, 9*(7), 676-682. doi:10.1038/nmeth.2019

Schroll, C., Riemensperger, T., Bucher, D., Ehmer, J., Voller, T., Erbguth, K., . . . Fiala, A. (2006). Light-induced activation of distinct modulatory neurons triggers appetitive or aversive learning in Drosophila larvae. *Curr Biol, 16*(17), 1741-1747. doi:10.1016/j.cub.2006.07.023

Schwaerzel, M., Monastirioti, M., Scholz, H., Friggi-Grelin, F., Birman, S., & Heisenberg, M. (2003). Dopamine and octopamine differentiate between aversive and appetitive olfactory memories in Drosophila. *Journal of Neuroscience, 23*(33), 10495-10502.

Sejourne, J., Placais, P. Y., Aso, Y., Siwanowicz, I., Trannoy, S., Thoma, V., . . . Preat, T. (2011). Mushroom body efferent neurons responsible for aversive olfactory memory retrieval in Drosophila. *Nat Neurosci, 14*(7), 903-910. doi:10.1038/nn.2846

Shah, S., & Hyde, D. R. (1995). Two Drosophila genes that encode the alph and beta subunits of the brain soluble guanylyl cyclase. *J Biol Chem, 270*(25), 15368-15376.

Shibuki, K., & Okada, D. (1991). Endogenous nitric oxide release required for long-term synaptic depression in the cerebellum. *Nature, 349*(6307), 326-328. doi:10.1038/349326a0

Shuai, Y., Lu, B., Hu, Y., Wang, L., Sun, K., & Zhong, Y. (2010). Forgetting is regulated through Rac activity in Drosophila. *Cell, 140*(4), 579-589. doi:10.1016/j.cell.2009.12.044

Skoulakis, E. M., Kalderon, D., & Davis, R. L. (1993). Preferential expression in mushroom bodies of the catalytic subunit of protein kinase A and its role in learning and memory. *Neuron, 11*(2), 197-208.

Stasiv, Y., Regulski, M., Kuzin, B., Tully, T., & Enikolopov, G. (2001). The Drosophila nitric-oxide synthase gene (dNOS) encodes a family of proteins that can modulate NOS activity by acting as dominant negative regulators. *J Biol Chem, 276*(45), 42241-42251. doi:10.1074/jbc.M105066200

Stuber, G. D., Hnasko, T. S., Britt, J. P., Edwards, R. H., & Bonci, A. (2010). Dopaminergic terminals in the nucleus accumbens but not the dorsal striatum corelease glutamate. *J Neurosci, 30*(24), 8229-8233. doi:10.1523/JNEUROSCI.1754-10.2010

Sulzer, D., Joyce, M. P., Lin, L., Geldwert, D., Haber, S. N., Hattori, T., & Rayport, S. (1998). Dopamine neurons make glutamatergic synapses in vitro. *J Neurosci, 18*(12), 4588-4602.

Sun, F., Zeng, J., Jing, M., Zhou, J., Feng, J., Owen, S. F., . . . Li, Y. (2018). A Genetically Encoded Fluorescent Sensor Enables Rapid and Specific Detection of Dopamine in Flies, Fish, and Mice. *Cell, 174*(2), 481-496 e419. doi:10.1016/j.cell.2018.06.042

Takemura, S. Y., Aso, Y., Hige, T., Wong, A., Lu, Z., Xu, C. S., . . . Scheffer, L. K. (2017). A connectome of a learning and memory center in the adult Drosophila brain. *Elife, 6*. doi:10.7554/eLife.26975

Tanaka, N. K., Tanimoto, H., & Ito, K. (2008). Neuronal assemblies of the Drosophila mushroom body. *J Comp Neurol, 508*(5), 711-755. doi:10.1002/cne.21692

Tang, S., & Yasuda, R. (2017). Imaging ERK and PKA Activation in Single Dendritic Spines during Structural Plasticity. *Neuron, 93*(6), 1315-1324 e1313. doi:10.1016/j.neuron.2017.02.032

Tecuapetla, F., Patel, J. C., Xenias, H., English, D., Tadros, I., Shah, F., . . . Koos, T. (2010). Glutamatergic signaling by mesolimbic dopamine neurons in the nucleus accumbens. *J Neurosci, 30*(20), 7105-7110. doi:10.1523/JNEUROSCI.0265-10.2010

Tempel, B. L., Bonini, N., Dawson, D. R., & Quinn, W. G. (1983). Reward learning in normal and mutant Drosophila. *Proc Natl Acad Sci U S A, 80*(5), 1482-1486.

Thurmond, J., Goodman, J. L., Strelets, V. B., Attrill, H., Gramates, L. S., Marygold, S. J., . . . FlyBase, C. (2019). FlyBase 2.0: the next generation. *Nucleic Acids Res, 47*(D1), D759-D765. doi:10.1093/nar/gky1003

Tomchik, S. M. (2013). Dopaminergic neurons encode a distributed, asymmetric representation of temperature in Drosophila. *J Neurosci, 33*(5), 2166-2176a. doi:10.1523/JNEUROSCI.3933-12.2013

Tomchik, S. M., & Davis, R. L. (2009). Dynamics of learning-related cAMP signaling and stimulus integration in the Drosophila olfactory pathway. *Neuron, 64*(4), 510-521. doi:10.1016/j.neuron.2009.09.029

Trannoy, S., Redt-Clouet, C., Dura, J. M., & Preat, T. (2011). Parallel processing of appetitive short- and long-term memories in Drosophila. *Curr Biol, 21*(19), 1647-1653. doi:10.1016/j.cub.2011.08.032

Tritsch, N. X., Ding, J. B., & Sabatini, B. L. (2012). Dopaminergic neurons inhibit striatal output through non-canonical release of GABA. *Nature, 490*(7419), 262-266. doi:10.1038/nature11466

Tully, T., & Quinn, W. G. (1985). Classical-Conditioning and Retention in Normal and Mutant Drosophila-Melanogaster. *Journal of Comparative Physiology a-Sensory Neural and Behavioral Physiology, 157*(2), 263-277. doi:Doi 10.1007/Bf01350033

Vanover, K. E., Davis, R. E., Zhou, Y., Ye, W., Brasic, J. R., Gapasin, L., . . . Wong, D. F. (2018). Dopamine D2 receptor occupancy of lumateperone (ITI-007): a Positron Emission Tomography Study in patients with schizophrenia. *Neuropsychopharmacology*. doi:10.1038/s41386-018-0251-1

Venken, K. J., Schulze, K. L., Haelterman, N. A., Pan, H., He, Y., Evans-Holm, M., . . . Bellen, H. J. (2011). MiMIC: a highly versatile transposon insertion resource for engineering Drosophila melanogaster genes. *Nature Methods, 8*(9), 737-743.

Vet, L. E. M., Vanlenteren, J. C., Heymans, M., & Meelis, E. (1983). An Air-Flow Olfactometer for Measuring Olfactory Responses of Hymenopterous Parasitoids and Other Small Insects. *Physiological Entomology, 8*(1), 97-106. doi:Doi 10.1111/J.1365-3032.1983.Tb00338.X

Walkinshaw, E., Gai, Y., Farkas, C., Richter, D., Nicholas, E., Keleman, K., & Davis, R. L. (2015). Identification of genes that promote or inhibit olfactory memory formation in Drosophila. *Genetics, 199*(4), 1173-1182. doi:10.1534/genetics.114.173575

White, N. M., & McDonald, R. J. (2002). Multiple parallel memory systems in the brain of the rat. *Neurobiol Learn Mem, 77*(2), 125-184. doi:10.1006/nlme.2001.4008

Wu, J. K., Tai, C. Y., Feng, K. L., Chen, S. L., Chen, C. C., & Chiang, A. S. (2017). Long-term memory requires sequential protein synthesis in three subsets of mushroom body output neurons in Drosophila. *Sci Rep, 7*(1), 7112. doi:10.1038/s41598-017-07600-2

Yakubovich, N., Silva, E. A., & O'Farrell, P. H. (2010). Nitric oxide synthase is not essential for Drosophila development. *Curr Biol, 20*(4), R141-142. doi:10.1016/j.cub.2009.12.011

Yamagata, N., Ichinose, T., Aso, Y., Placais, P. Y., Friedrich, A. B., Sima, R. J., . . . Tanimoto, H. (2015). Distinct dopamine neurons mediate reward signals for short- and long-term memories. *Proc Natl Acad Sci U S A, 112*(2), 578-583. doi:10.1073/pnas.1421930112

Zars, T., Fischer, M., Schulz, R., & Heisenberg, M. (2000). Localization of a short-term memory in Drosophila. *Science, 288*(5466), 672-675.

Figures legends

Figure 1. Dopaminergic neurons can induce memories without dopamine, but with opposite valence

(A) Conceptual diagram of the circuit organization in the MB lobes. Sparse activity in the parallel axonal fibers of the KCs represent odor stimuli. DAN inputs induce plasticity at KC to MBON synapses (represented by circles), when DAN and KC activity are coincident (red circles). The MB compartments (indicated by the colored rectangles) differ in their learning and memory decay rates. The actual MB contains 15 compartments (Tanaka et al., 2008).

(B) Top: Design of the optogenetic olfactory arena and a diagram illustrating odor paths in the arena. (C) Schematic representation of the innervation patterns of the PPL1 (blue; *R52H03-p65ADZp; TH-ZpGAL4DBD*) and PAM cluster (orange; *R58E02-p65ADZp; DDC-ZpGAL4DBD*) dopaminergic neurons used to train flies. A diagram of the training protocol is also shown. Flies were trained and tested in the olfactory area. A 1-min odor exposure was paired with thirty 1-s pulses of red light (627 nm peak and 34.9 $\mu W/mm^2$), followed by 1-min without odor or red light, and then presentation of a second odor for 1-min without red light. In one group of flies, odors A and B were 3-octanol and 4-methylcyclohexanol, respectively, while in a second group of flies, the odors were reversed. Memory was tested immediately after three repetition of training bouts by giving flies a binary choice between the two odors in the olfactory area.

(D-G) Odor memories induced by the collective optogenetic activation of PPL1-γ1pedc, PPL1-γ2α'1, PPL1-α'2α2 and PPL1-α3 DANs (upper panels; blue lines) or activation of PAM cluster DANs (lower panels; orange lines) in wild type (D), TH mutant (E), TH mutant with feeding of 1mg/ml L-DOPA and 0.1mg/ml carbidopa (F), or TH mutant with

cell-type specific expression of a wild-type TH cDNA (G; see the methods for drug treatment and supplemental information for genotypes). Time courses of the performance index (PI) during the test period are shown as the average of reciprocal experiments. The PI is defined as [(number of flies in the odor A quadrants) - (number of flies in odor B quadrants)]/(total number of flies). Thick line and shading represent mean ± SEM. N= 12-16. Two split-GAL4 drivers R52H03-p65ADZp in attP40; TH-ZpGAL4DBD in VK00027 and R58E02-p65ADZp in attP40; DDC-ZpGAL4DBD in VK00027 were used for driving 20xUAS-CsChrimon-mVenus in PPL1 or PAM DANs, respectively.

Figure 1-figure supplement 1 Cell type specific rescue of TH

TH immunoreactivity (from left to right): PAM DANs in wild type; PAM DANs in TH mutant; PAM DANs in TH mutant with cell-type specific rescue of TH using UAS-TH; PPL1 DANs in TH mutant; and or PPL1 DANs in TH mutant with cell-type specific rescue of TH using UAS-TH. In the TH mutant background, TH immunoreacivity in the brain was completely abolished, except for a few cells dorsal medial surface of the brain and near the ventral lateral protocerebram (arrow heads). With UAS-TH, TH immunoreactivity was restored in PAM or PPL1 DANs (arrows). The expression pattern, visualized using UAS-CsChrimson-mVenus, of the PAM and PPL1 drivers used is shown in lower panels.

Figure 2. Cotransmitter effects differ among DAN cell types

The PI of olfactory memories measured immediately after 3x 1-min training in TH mutant/TH+ heterozygotes (+) or TH mutant/TH mutant (-) background. Odor presentation was paired with either activation of bitter taste neurons (Gr66a-GAL4) or

the indicated subset of DANs in which optogentic activation was used as diagramed in Figure 1C. A split-GAL4 driver without enhancer (empty) was used as a control. The bottom and top of each box represents the first and third quartile, and the horizontal line dividing the box is the median; the PI was calculated by averaging the PIs from the final 30 s of each test period (see legend to Figure 1). The whiskers represent the minimum and maximum. N= 8-16. Asterisk indicates significance from the empty-GAL4 control. Comparison with chance level (i.e. PI=0) resulted in identical statistical significance: *, $p < 0.05$; **, $p < 0.01$; ***, $p < 0.001$; n.s., not significant. See Figure S2 and www.janelia.org/split-gal4 for expression patterns of split-GAL4 drivers.

Figure 2-figure supplement 1 Expression patterns of driver lines

Expression patterns of CsChrimson-mVenus driven by denoted split-GAL4 drivers made in this study. All other lines used were reported previously. See supplemental table 1 for the list of driver lines and Aso et al. 20114a and www.janelia.org/split-gal4 for primary image data of other split-GAL4 lines.

Figure 3 Identification of NOS1 in PPL1-γ1pedc and PAM- γ5 by RNA-Seq

(A) The RNA-Seq data of two cell types that showed the valence-inversion phenotype (i.e. PPL1-γ1pedc and PAM- γ5) were pooled and compared against the pooled data of all other cell types examined (DANs, MBONs, KCs). The $-\log_{10}$ of p-values for comparing number of counted transcripts between the pooled data of PPL1-γ1pedc and PAM- γ5 relative to that of all other cell types were plotted against the $\log_2$ of fold changes

observed in the expression levels of transcripts. Different splice isoforms of genes are plotted separately (dots). Green dots represent the 2,981 transcripts expressed at levels above 10 transcripts per million (TPM) in both PPL1-γ1pedc and PAM-γ5. Gray dots represent the 31,539 transcripts with expression levels below 10 TPM in one or both of these two DANs. Dots on +20 or -20 x-axis represent splice isoforms that were dected only in the PPL1-γ1pedc and PAM- γ5 or other cell types. Magenta dots show the three splice isoforms of NOS.

(B) Mean TPM of NOS splicing isoforms. The magenta dashed line highlights PPL1-γ1pedc and PAM- γ5, the two cell types that showed the valence-inversion phenotype.

(C) Map of the NOS locus. Exons and protein coding sequences are dipicted as boxes and gray boxes, respectively. Only the full length isoform NOS-RA (dNOS1) produces a functional NOS protein (Stasiv et al., 2001). The antibody we used was raised against exon16 (Kuntz et al., 2017; Yakubovich et al., 2010). Arrows indicate the first four exons of NOS1 and NOS4 where 40 FISH probes were designed to recognize these, but not NOS-RK transcripts. See Methods for details of the position and sequence of the probes.

(D) NOS immunoreactivity was observed in the γ1pedc compartment of the MB. Immunoreactivity was markedly reduced by expressing NOS-RNAi in PPL1-γ1pedc.

(E) Distribution of NOS-immunoreactivity inside the MB is displayed. Voxels above mean +2SD of the entire brain are shown in 12 bit scale in magenta. Insert shows a quantification of NOS-immunoreactivity in each MB compartment. Signal in γ1 was significantly higher than 12 compartments indicated by the bracket (Kruskal-Wallis

with Dann's test for selected pairs). Signal in γ1 was significantly higher than 8 compartments indicated by the bracket; *, $p < 0.05$; **, $p < 0.01$; n=12

Figure 3-figure supplement 1 Controls for RNA-Seq reproducibility, anti-NOS antibody specifity and FISH probes.

(A) Relationship between cDNA yields, number of sorted cells, mapped reads, number of detected genes with more than one mapped read. Data for each biological replicate are shown. Original data are presented in Supplementary File 1.

(B) Quantification of NOS immunoreactivity (a.u.; arbitrary units) in the γ1 or α2 compartment with or without NOS-RNAi. The whiskers represent the minimum and maximum. N= 12. Asterisk indicates significance from 0: *, $p < 0.05$; n.s., not significant. Horizontal dotted line indicates mean NOS signals in the brain.

(C) Outside of the MB, only a couple of additional DANs that are labeled by the NOS FISH probes. Colabelling by FISH probes against TH (green) and first 4 exons of NOS1 transcripts (magenta) is shown. Diagram and projection of anterior or posterior brains are shown. Circles in diagram represent soma of DANs detected by TH probes; the different clusters of dopaminergic cell bodies (PAM, PAL, T1, PPM1, PPM2, PPM3, PPL1, PPL2c, PPL2ab and VUM) are labeled. Circles filled with magenta represent DANs overlapping with NOS (arrows). In addition to one cell in PPL1 (presumably PPL1- γ1pedc) and about a dozen of PAM cluster cells, we observed that one cell in the PPL2ab cluster and a small TH-positive cell outside, but near, the PPL2ab cluster (arrows) were labeled with NOS-FISH probes.

(D) NOS-FISH signal was observed in soma of PPL1-γ1pedc but not in PPL1-α′2α2.

Figure 3-figure supplement 2 RNA-seq data for genes related to neurotransmitters

Mean TPM values for each gene isoform are listed with the corresponding gene ID. See Supplementary File 1 for the full data set.

Figure 4 NOS in dopaminergic neurons contributes to memory formation.

(A) Increasing the dose of L-NNA reduced the positive-valence memory induced by activation of PPL1-γ1pedc in a TH mutant background. The ability to form an negative-valence memory was restored by feeding of L-DOPA plus cardidopa and this memory formation was not affected by L-NNA. N=8-12.

(B) Feeding of L-NNA in a TH mutant background reduced the negative-valence memory induced by activation of the combination of PAM- γ5 and PAM-β′2a, but not of PPL1- γ2α′1. N= 12-16

(C) Activation of PPL1 DANs (PPL1-γ1pedc, PPL1-γ2α′1, PPL1-α′2α2 and PPL1-α3) induced significant positive-valence memory in TH mutant background. The valence of the induced memory was negative when NOS-RNAi was expressed in the same DANs. We postulate that the negative-valence memory observed when NOS-RNAi is expressed results from an as yet unidentified cotransmitter released by PPL1-γ2α′1 (see also panel B and Figure 2). N= 8

(D) NOS immunoreactivity in the α3 compartment in wild type (left) and after ectopic

expression of NOS (right).

(E) Activation of PPL1-α3 with ectopic expression of NOS induced significant positive-valence memory after 3x 1-min training protocol in TH mutant background (Figure 1C). Note that activation of PPL1-α3 can induce negative-valence memory in wild-type background, but only after 10x spaced training (Aso & Rubin, 2016). N= 12

In A-C and E, memories assessed immediately after 3x 1-min training are shown. The bottom and top of each box represents the first and third quartile, and the horizontal line dividing the box is the median. The whiskers represent the minimum and maximum. N= 8-16. Asterisk indicates significance of designated pair in A and B, or from 0 in C and D: *, $p < 0.05$; ***, $p < 0.001$; n.s., not significant.

Figure 5 Soluble guanylate cyclase in the Kenyon cells is required to form NO-dependent memory

(A) Diagram of soluble or receptor guanylyl cyclases in Drosophila.

(B) RNA-seq data indicate coexpression of Gycα99B and Gycβ100B in KCs, MBONs and DANs. For comparison, other guanylate cyclase are also shown. Note that RNA-Seq detected transcripts of neuropeptide gene Nplp1 in both PPL1-γ1pedc and PAM-γ5 (Figure S4), but expression of its receptor Gyc76C was barely detectable compared to Gycα99B and Gycβ100B.

(C) Induction of Gycβ100B-shRNA in Kenyon cells by activating MB247-switch driver (Mao, Roman, Zong, & Davis, 2004) with RU-486 feeding reduced the positive-valence

memory induced by PPL1-γ1pedc. We also observed a partial effect in the flies without RU-486, presumably due to leaky expression. Negative-valence memory with additional feeding of L-DOPA and cardidopa was not affected by Gycβ100B-shRNA induction in KCs. Memories immediately after 3x 1-min training are shown. The bottom and top of each box represents the first and third quartile, and the horizontal line dividing the box is the median. The whiskers represent the minimum and maximum. N= 12-16. Asterisk indicates significance of designated pair: *, $p < 0.05$; **,$p < 0.01$; n.s., not significant.

Figure 5-figure supplement 1

Expression of Gycbeta100B in the mushroom body lobes

Distribution of Gycbeta100B-EGFP in flies carrying the Gycbeta100B[MI08892-GFSTF.2] in the mushroom body lobes is shown with anterior to posterior confocal sections. Right panels show images of wild-type fly, which did not contain the Gycbeta100B-EGFP insertion, prepared with the identical immunolabelling procedure.

Figure 6 NO-dependent effect develops slowly, requires longer training than dopamine-dependent memory, and shortens memory retention

(A) Schematic diagram of training protocols.

(B) Learning rate by activation of PPL1-γ1pedc in wild type (left; blue), wild type with L-NNA feeding (center; purple) or TH mutant background (right; blue). Memory scores were not significantly affected by L-NNA feeding in any of the training protocols in wild type

flies. A single 10-s training was insufficient to induce any detectable memory in TH mutant background, but induced significant negative-valence memory in wildtype background. (C) Time course of NO-dependent, positive-valence memory induced by PPL1-γ1pedc in a TH mutant background after 1x 1-min training. Data point and error bars indicate mean and SEM. N=8-10. Note that the plot is split in the time axis to better display the kinetics.

(D) After 1x 1-min training, a cell type specific knock down of NOS in PPL1-γ1pedc prolonged the retention of negative-valence memory induced by PPL1-γ1pedc in wild-type background measured at 3 and 6 hours. Note that expression of NOS-RNAi did not affect the score of immediate memory. N= 12.

(E) Effect of repetitive trainings on 1-day memory. Repetitive training with activation of PPL1-γ1pedc did not induced significant 1-day memory in wild-type background irrespective of training protocols (blue; left). Flies expressing NOS-shRNA showed significant 1-day memory after 10x spaced training (purple; center). In a TH mutant background (right), appetitve memory was induced by 3X and 10X repetitive training. For activation of PPL1-γ1pedc, VT045661-LexA was used as the driver for experiments in B, C and TH mutant background data in E, and MB320C split-GAL4 for wild-type and NOS-RNAi data in D. We made consistent observations with both global L-NNA inhibition of NOS and cell-type-specific NOS-RNAi (see Figure S6). The bottom and top of each box represents the first and third quartile, and the horizontal line dividing the box is the median. The whiskers represent the minimum and maximum. N= 12-16. Asterisk indicates significance between control and NOS-RNAi in D, between designated pair in E, or from 0 in all others: *, $p < 0.05$; **,$p < 0.01$; ***,$p < 0.001$; n.s., not significant.

Figure 6-figure supplement 1

(A) L-NNA feeding prolonged retention of memory induced by 1x 1-min training with PPL1-γ1pedc activation at 3 and 6 hour time points. VT045661-LexA was used as a driver to express CsChrimson-mVenus. Data point and error bars indicate mean and SEM. *, $p < 0.05$; **,$p < 0.01$

(B) Knockdown of NOS in PPL1-γ1pedc prolonged memory retention after 1x 1-min training with 60V electric shock. N=12.

(C) Inhibition of NOS by L-NNA prolonged the retention of memory that was induced by 10x spaced training with activation of PPL1-γ1pedc using the VT045661-LexA driver. N=12. The bottom and top of each box represents the first and third quartile, and the horizontal line dividing the box is the median. The whiskers represent the minimum and maximum. *, $p < 0.05$

Figure 7 Nitric oxide enhances fast update of memory

(A) Experimental design to measure dynamics of memory when flies encounter new experiences after establishing an initial odor memory that was induced by the 3x 1-min spaced training that paired odor presentation with optogenetic PPL1-γ1ped activation .

(B) In reversal learning, the control odor in the first three trainings was now paired with activation of PPL1-γ1ped. In all three cases, the first reversal learning was sufficient to modify the odor preference. However, only in wild-type flies was this change large enough that the flies prefered the new odor. In L-NNA fed or TH mutant (dopamine

deficient) flies changing the odor preference required multiple training sessions with the new odor.

(C) Three exposures to each of the two odors did not significantly change the odor preference in any of the three sets of flies.

(D) One activation of PPL1-γ1ped without odor quickly reduced conditioned response in wild type. L-NNA fed flies or dopamine deficient flies required three or five times, respectively, more repetitions of PPL1-γ1ped activation to significantly reduce the conditioned response.

(E) Changes in PI induced by 3x training (as measured in Test 2) resulting from the first reversal training (left) or from DAN activation without odor presentation (right) (as measured in Test3). The observed changes were significantly larger in wild-type flies compared to L-NNA fed flies.

Figure 8 Modeling dopamine and NO mediated plasticity

(A) Summary of plasticity model for independent DA and NO pathways. Synaptic weight w_i from KC_i to an MBON is increased or decreased depending on the pairing protocol. *A* and *B* determine the magnitude of the depression or potentiation induced by pairing, and τ determines the timescale over which weight changes occur.

(B) Illustration of the effects of the model in (A), for only DA (left) or only NO (right) dependent plasticity. In each plot, KC and DANs are first co-activated, followed by a later DA activation without KC activation.

(C) Model performance index (PI) for different pairing protocols. In (C)-(F), crosses represent the means of data from Figure 7.

(D) Modeling effects of combined DA and NO dependent plasticity. Gray curve: synaptic weights *w(t)* are modeled as an additive function of DA and NO dependent effects *D(t)* and *N(t)*, $w(t) \propto N(t) - D(t)$. Blue curve: a multiplicative interaction with $w(t) \propto (1 + N(t))\ (1 - D(t))$.

(E) Modeling 24-hour memory decay following 1x1-min odor pairing. We assume a low level of spontaneous DAN activity and choose B_{DA} and B_{NO} to fit the data. Blue curve: control. Purple curve: only DA dependent plasticity (compared to data from NOS-RNAi experiment).

(F) Modeling effects of DAN activation and reversal learning. B_{DA} and B_{NO} are chosen to fit the effects of DAN activation (top). The model qualitatively reproduces the effects of reversal learning (bottom) with no free parameters.

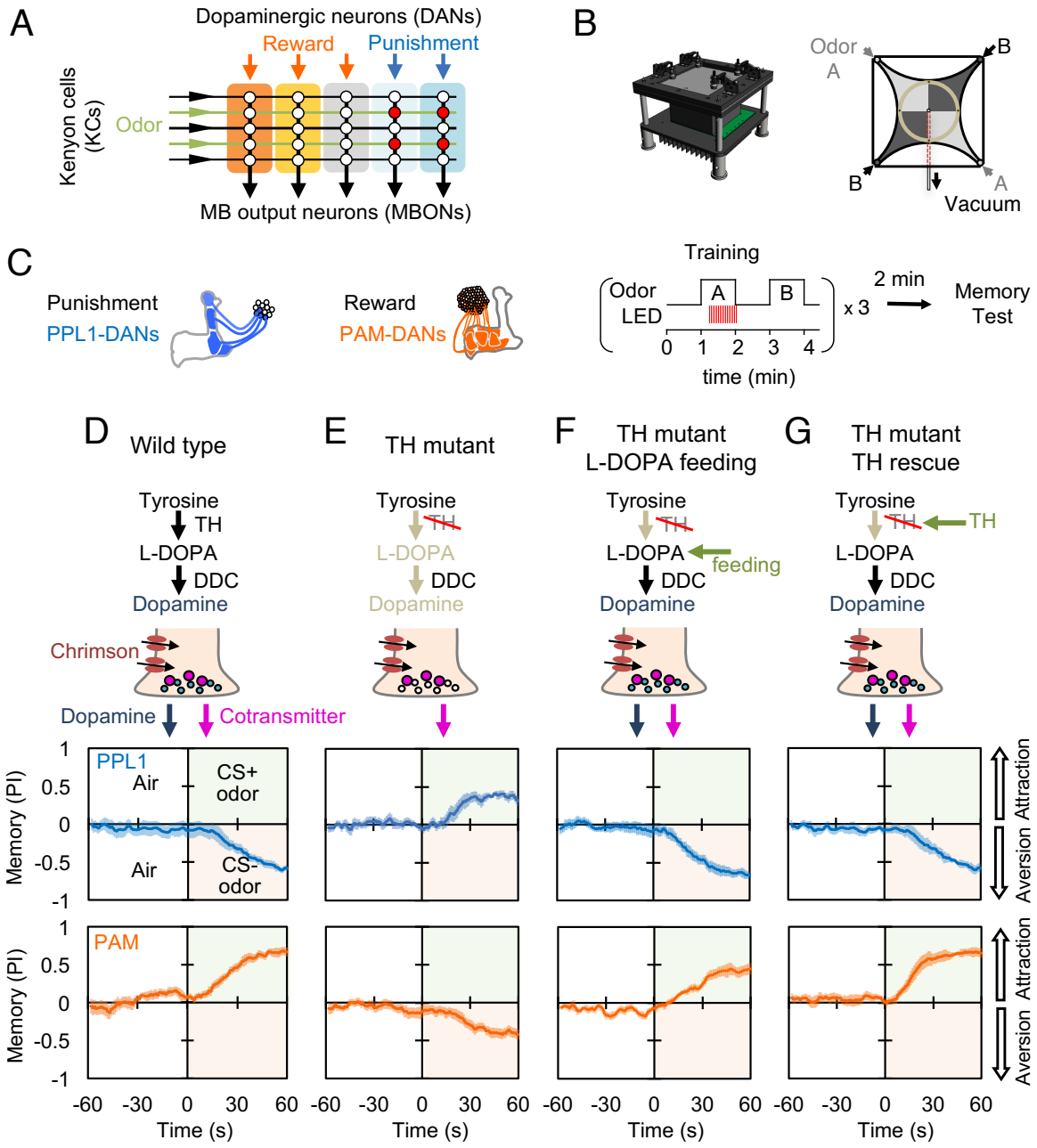

Figure 1

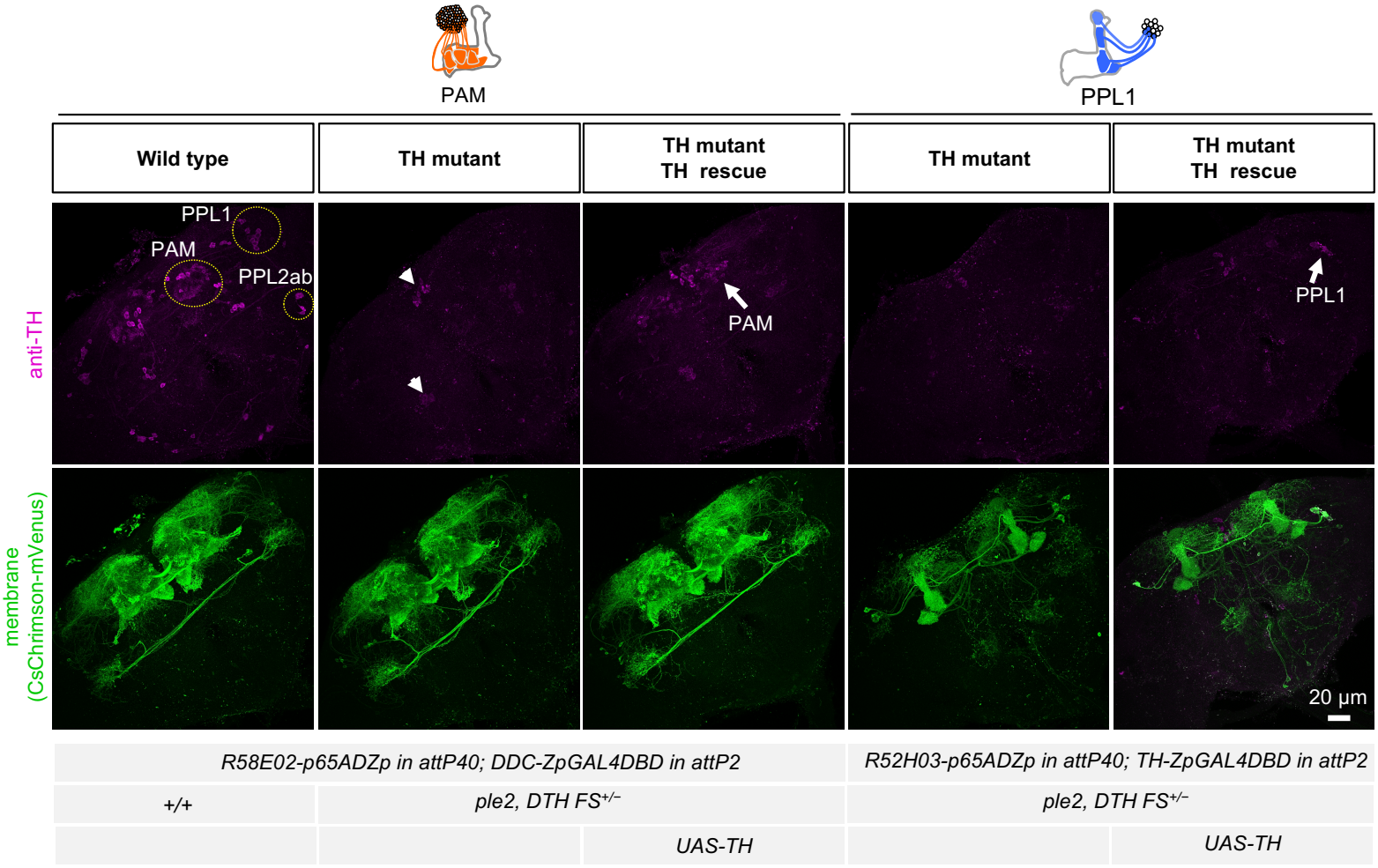

Figure 1 - figure supplement 1

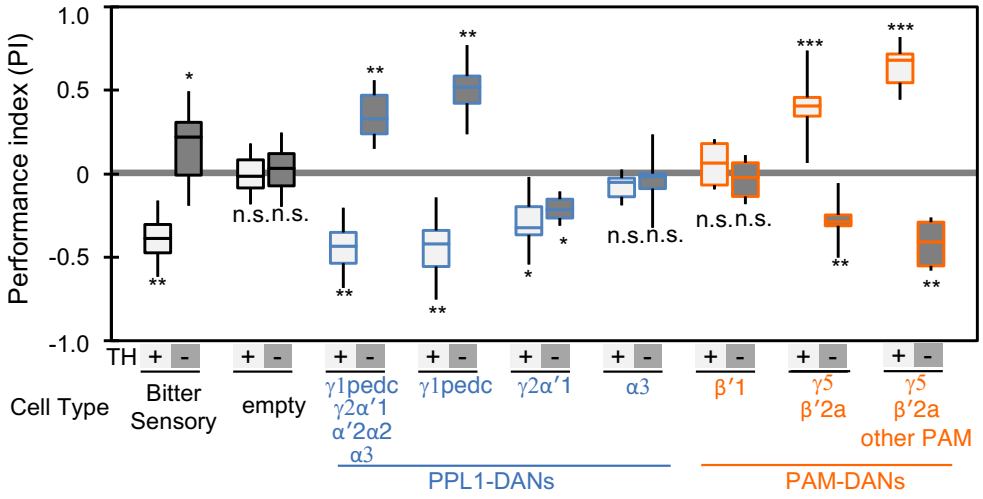

Figure 2

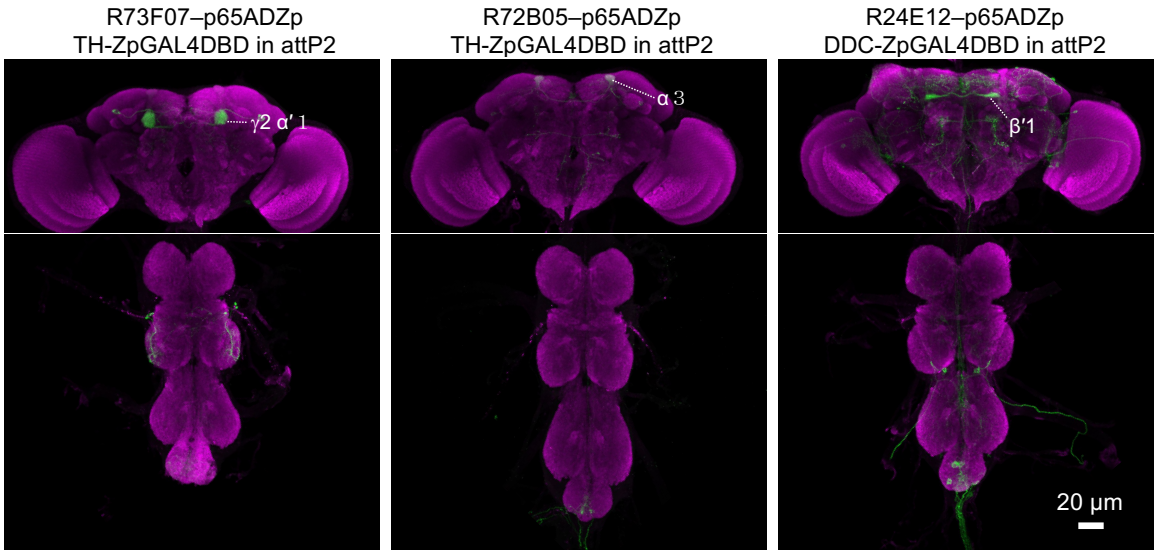

Figure2 - figure supplement 1

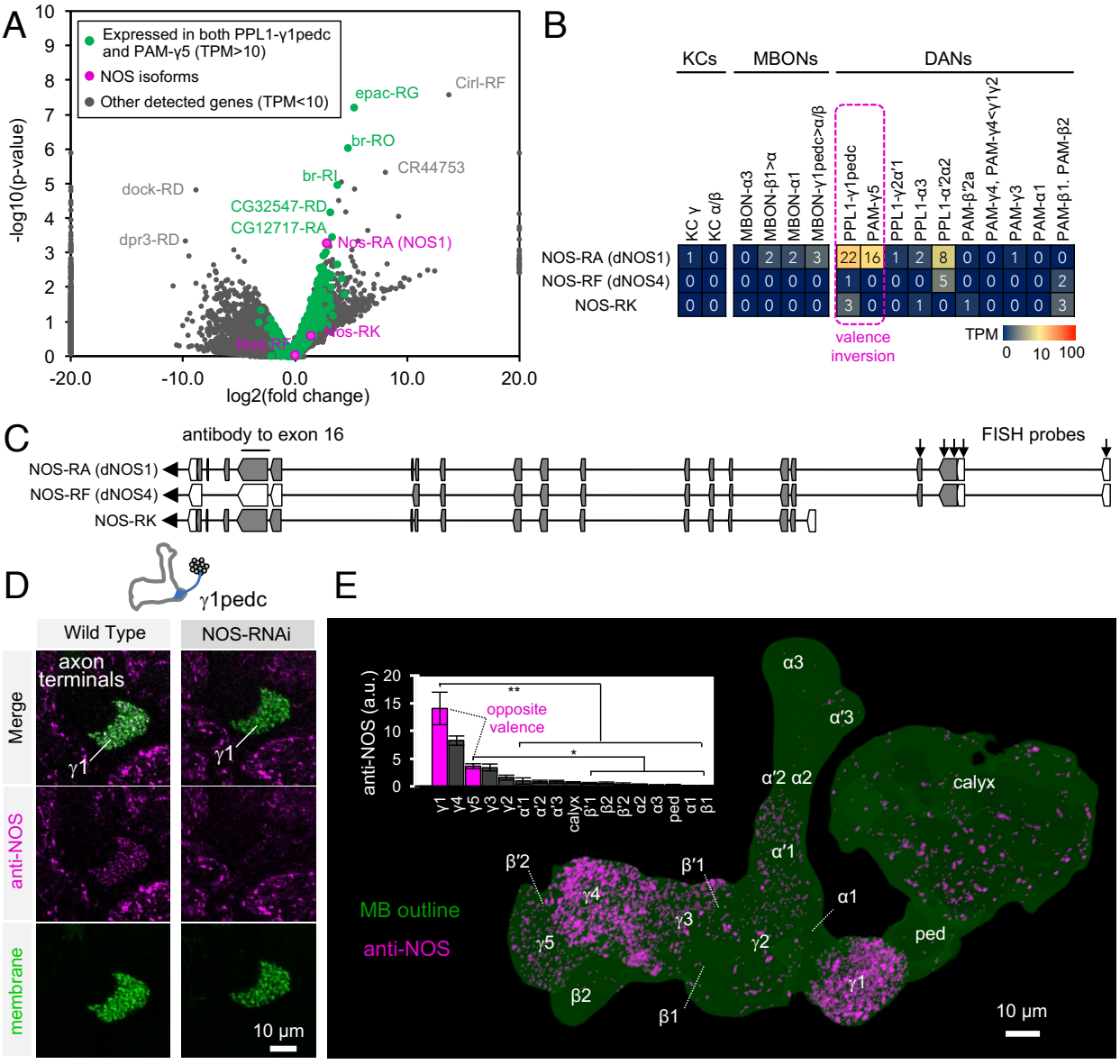

Figure 3

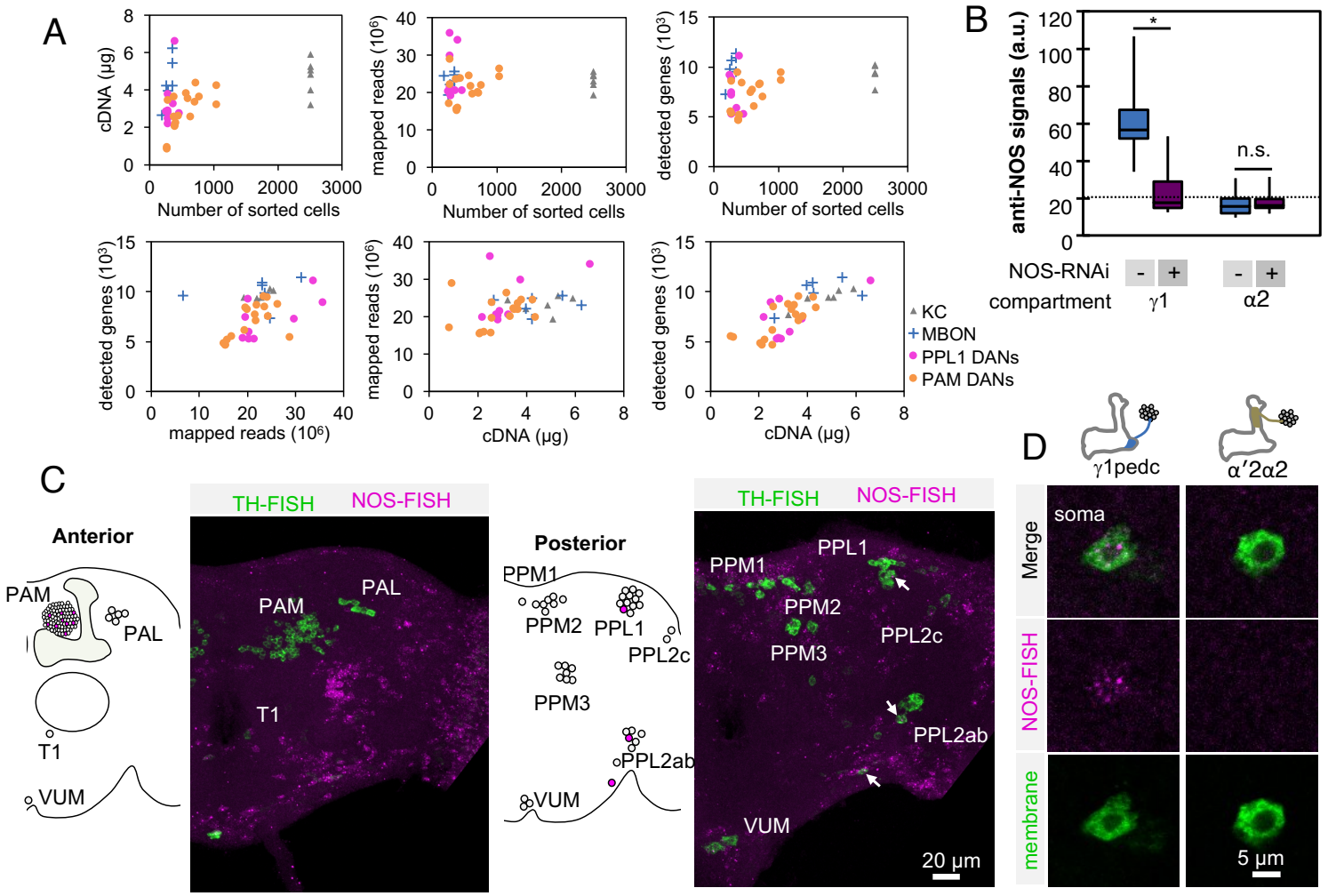

Figure 3- figure supplement 1

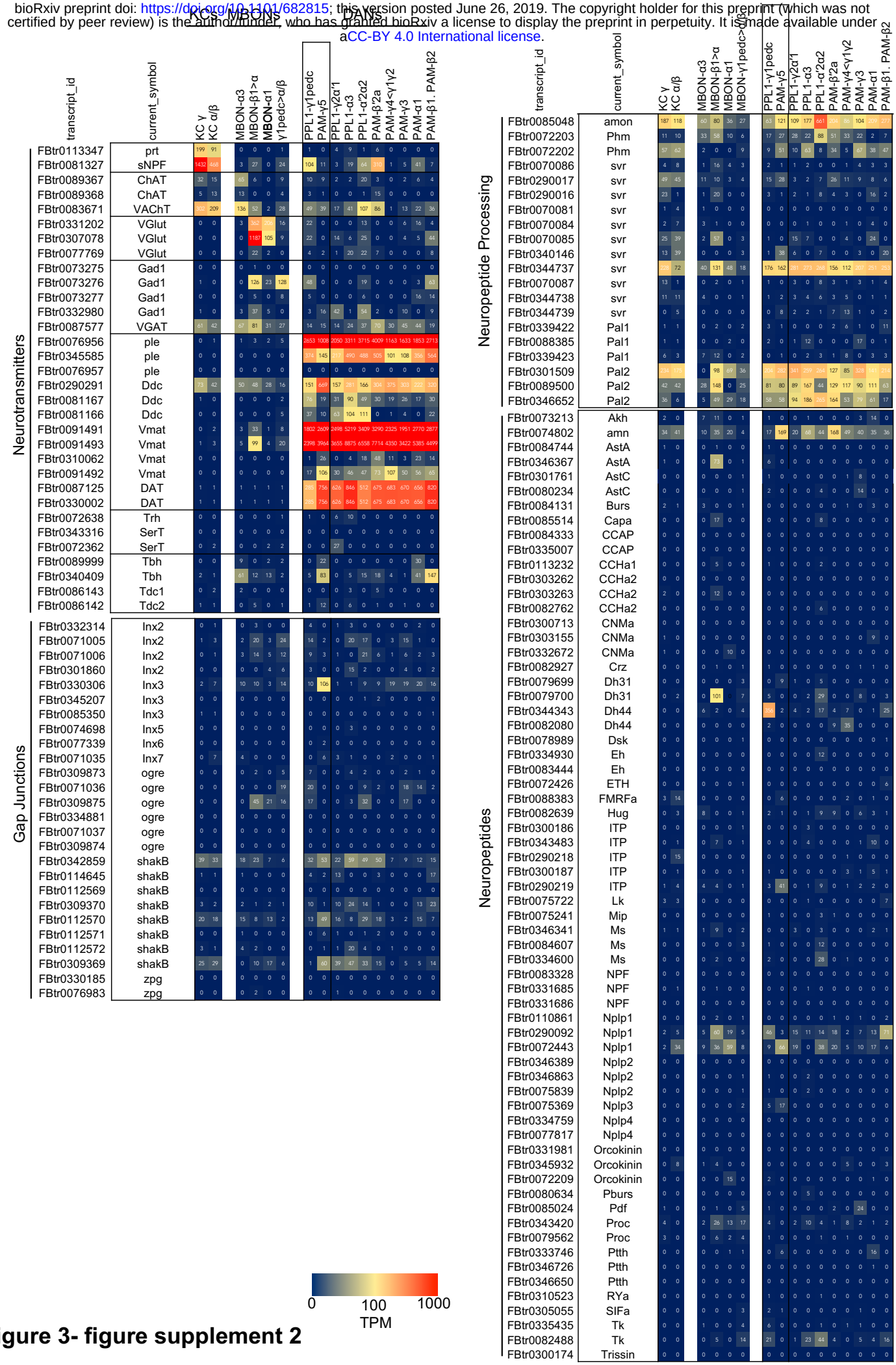

Figure 3- figure supplement 2

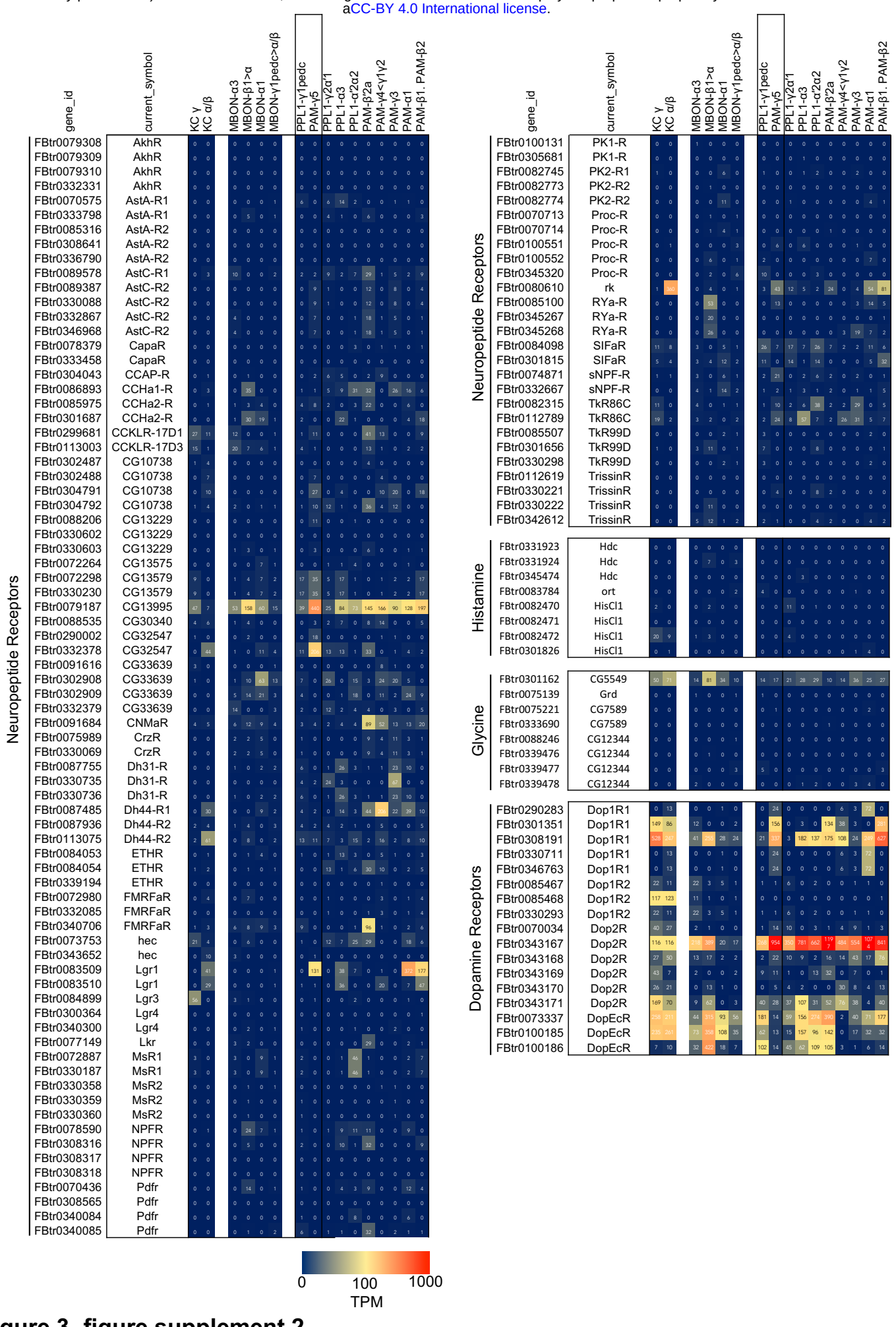

Figure 3- figure supplement 2

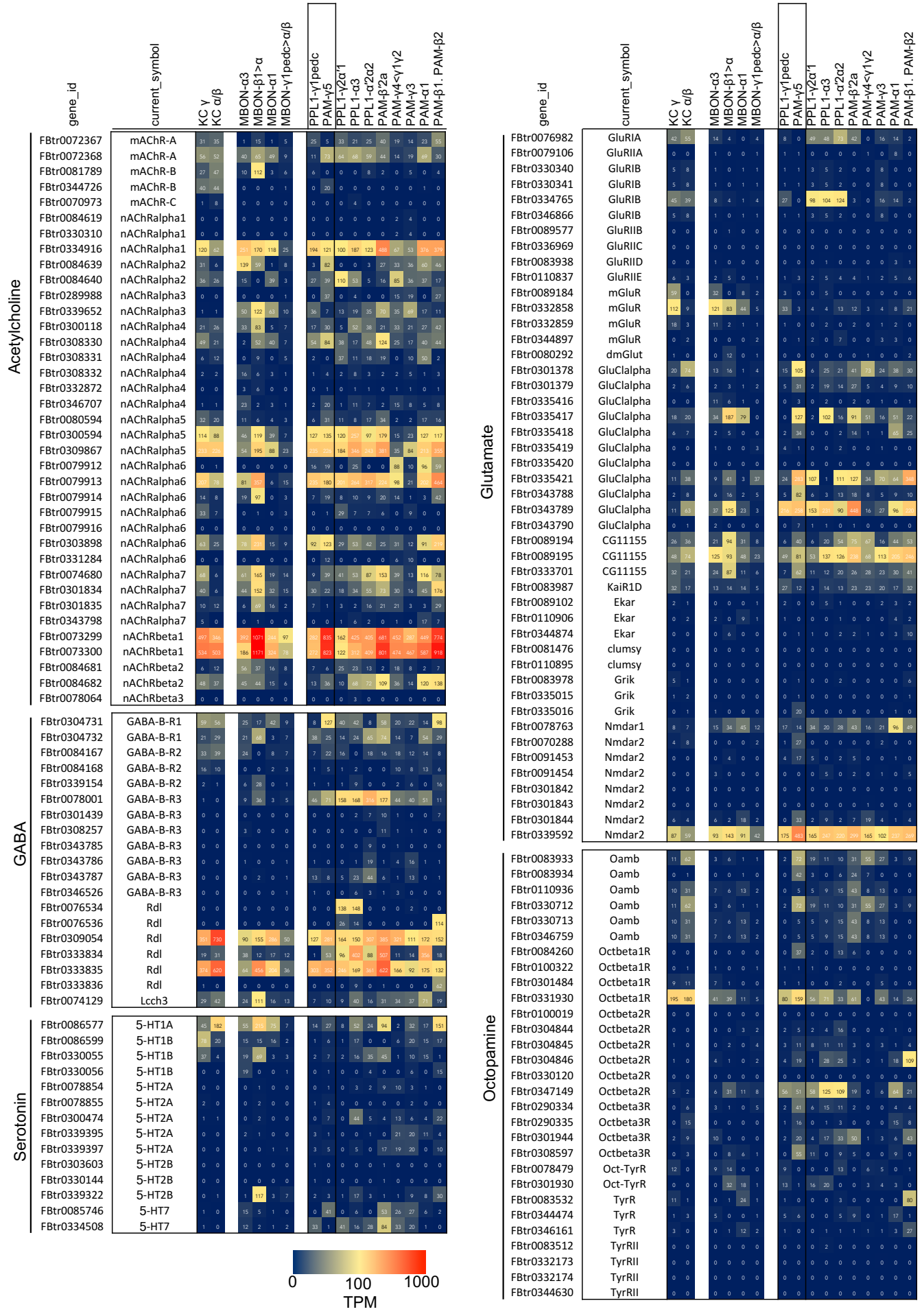

Figure 3- figure supplement 2

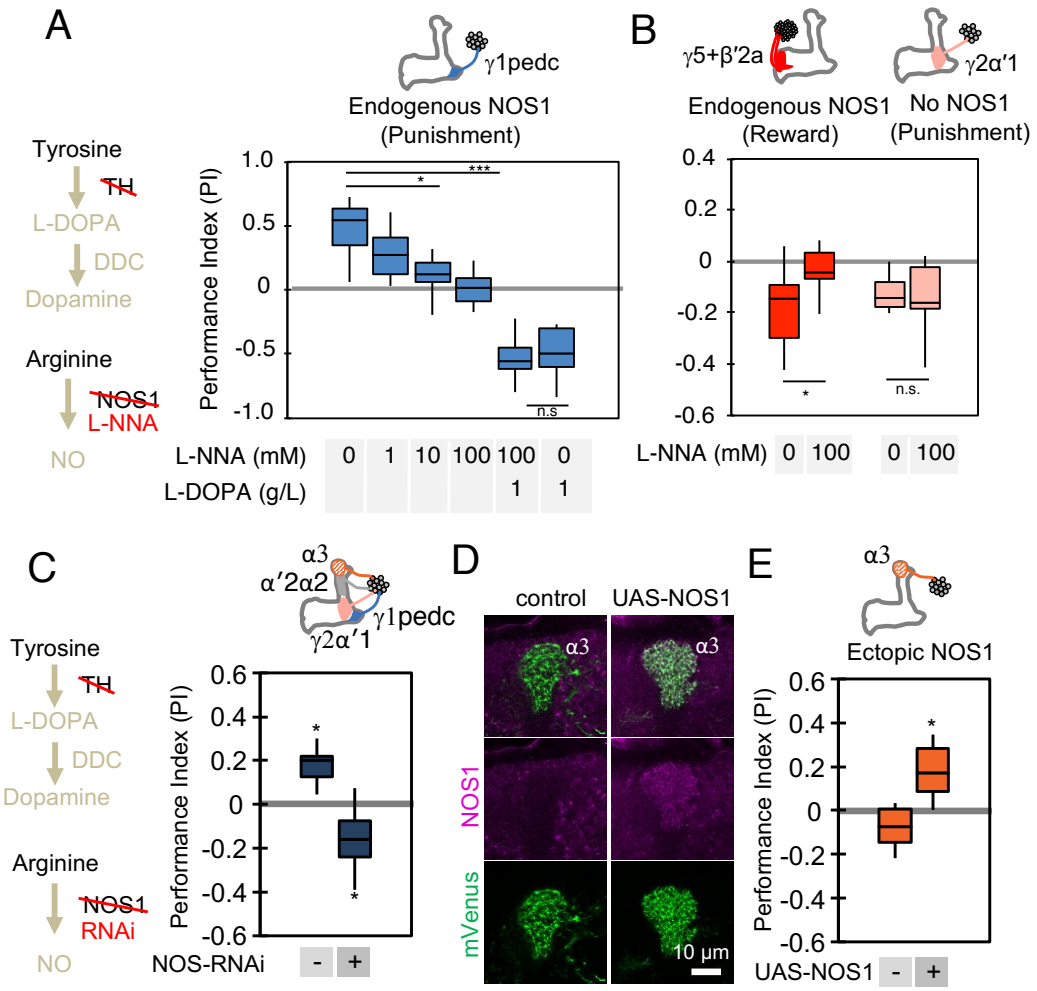

Figure 4

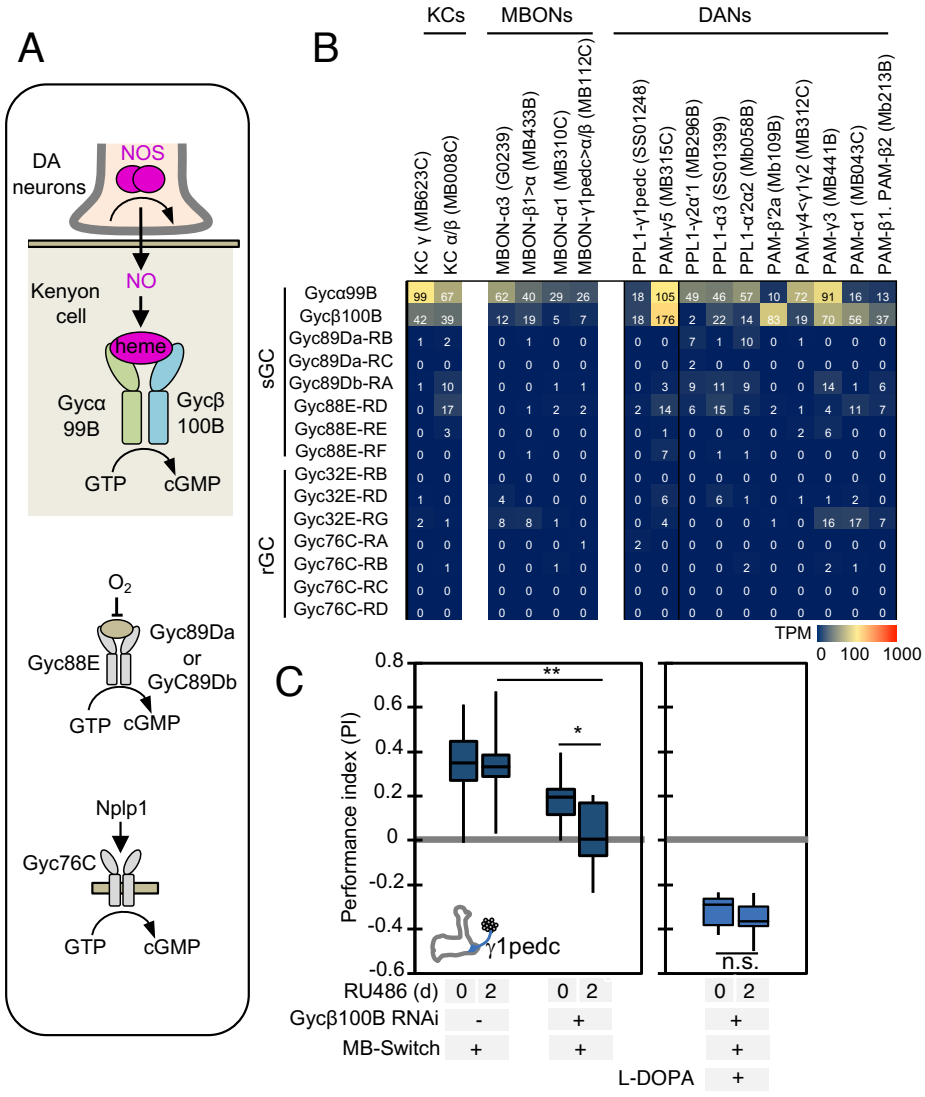

Figure 5

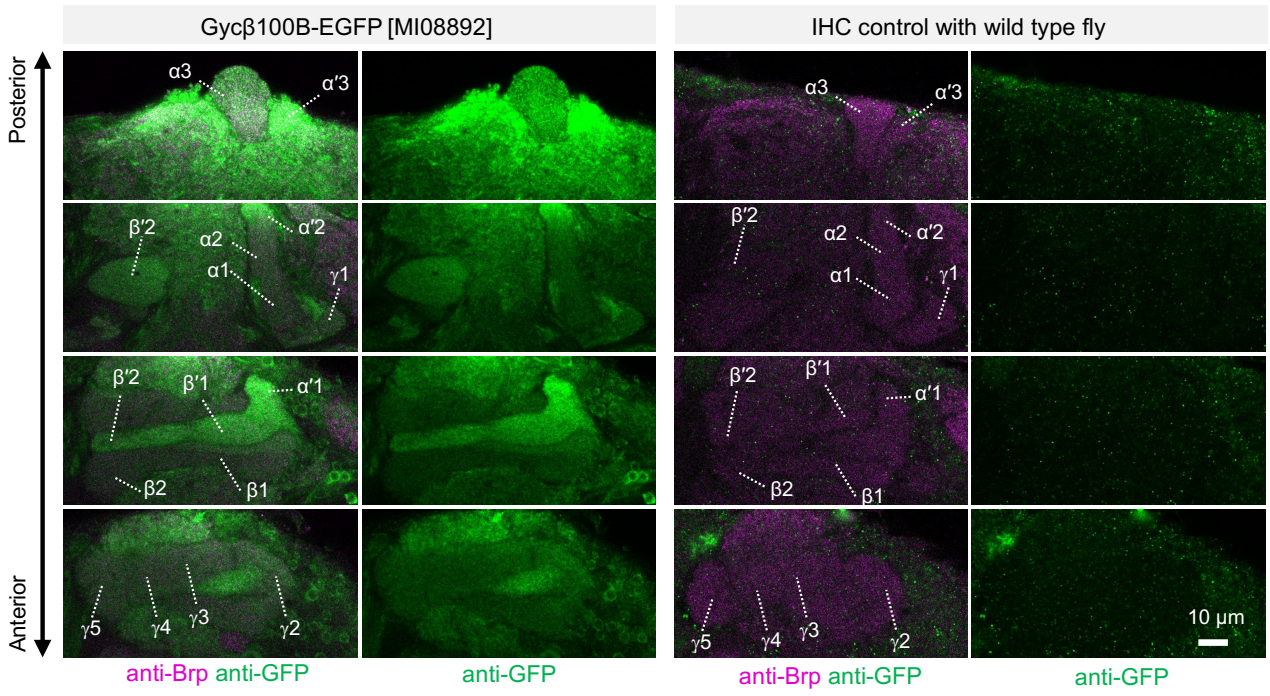

Figure 5- figure supplement 1

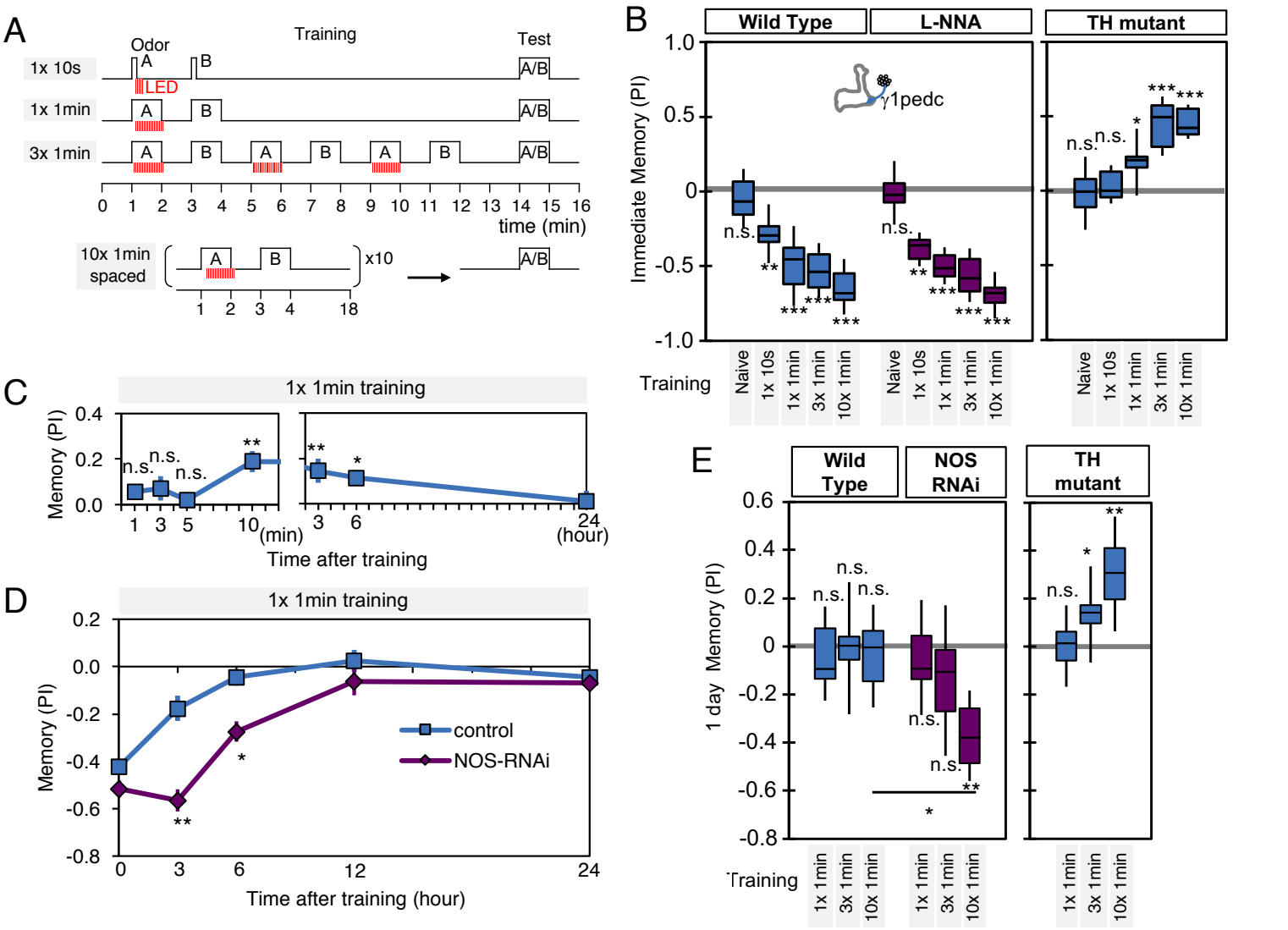

Figure 6

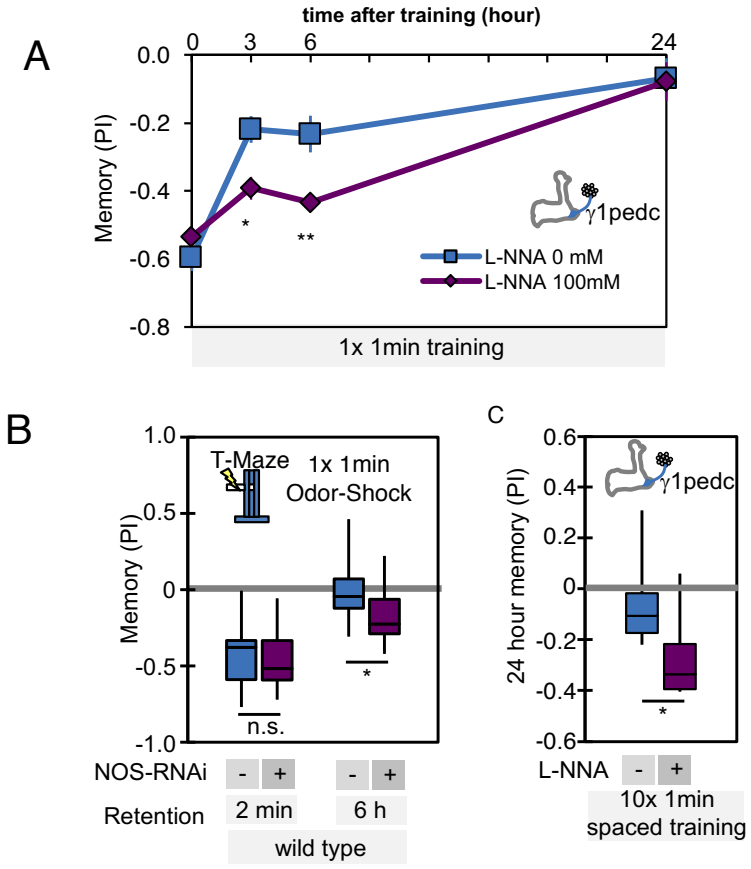

Figure 6- figure supplement 1

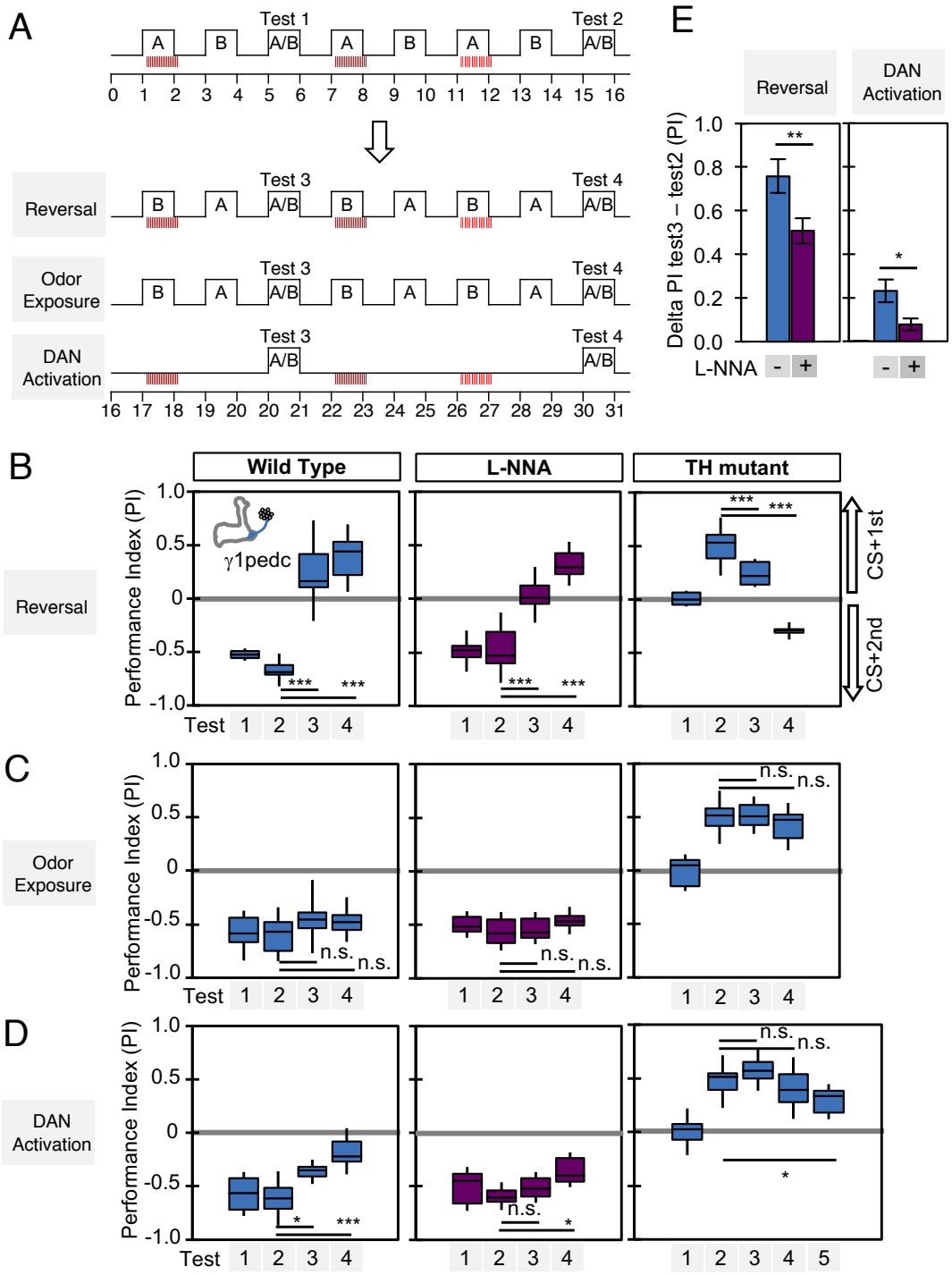

Figure 7

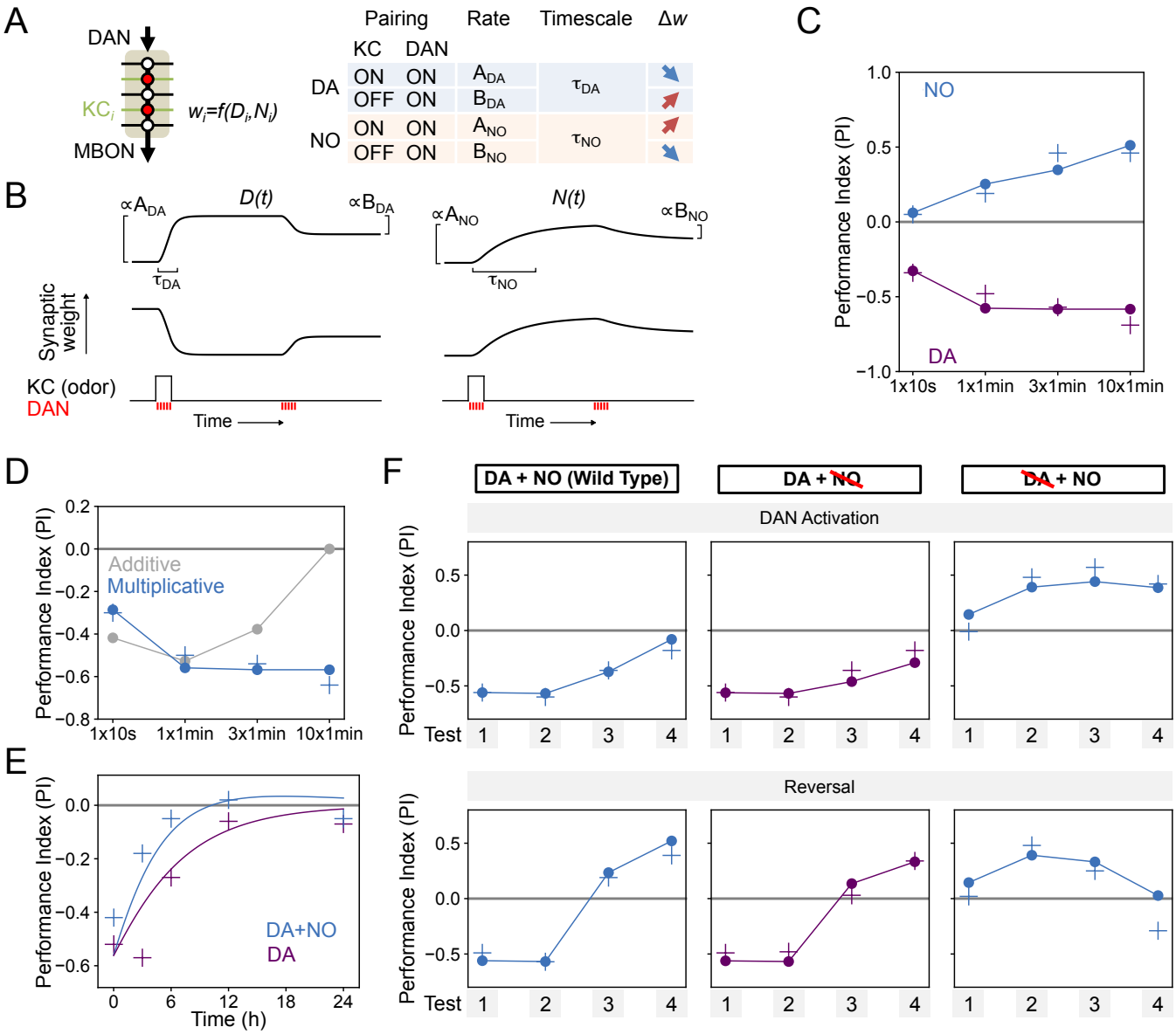

Figure 8